www.ijprems.com
editor@ijprems.com

INTERNATIONAL JOURNAL OF PROGRESSIVE RESEARCH IN ENGINEERING MANAGEMENT AND SCIENCE (IJPREMS)

Vol. 02, Issue 09, September 2022, pp : 01-25

e-ISSN : 2583-1062

Impact Factor : 2.265

# EFFECT OF TEXTURE ON THE BEHAVIOUR OF HYDRODYNAMIC JOURNAL BEARING

**L.Roy[1], Rohit Sharma[2], Suhel Yasir[3], Gautam Das[4], Mantu Gupta[5], Jayanta Gogoi[6]**

[1,2,3,4,5,6]Department of Mechanical Engineering, National Institute of Technology Silchar, Assam, India

[1]Corresponding Author: lintu2003@gmail.com

## ABSTRACT

Design of smart journal-bearing systems is an important issue that opens up the possibility for semi active dynamic control of bearing behaviour. A growing interest is given to the textured hydrodynamic lubricated contacts. The use of textured surfaces with different shapes of micro cavities (textures) and at different locations of the texture zone can be an effective approach to improve the performance of bearings. The present study examines the effect of different shape textures on the performance hydrodynamic journal bearing. A numerical modelling is used to analyze the different types of texture effect on the characteristics of a hydrodynamic journal bearing using Matlab. The theoretical results show that the most important characteristics can be improved through an appropriate arrangement of the textured area on the contact surface. CFD Analysis is also performed with the help of three different shapes of textures using the ANSYS Fluent CFD Software. The CFD results shows that the load carrying capacity of the bearing increases with the surface textures and the optimal arrangement of the textures and their types is of crucial importance for a high-performance bearing.

**Keywords:** Textures, Hydrodynamic lubrication, Journal bearing, Finite difference method, CFD (Computational Fluid Dynamics), Load carrying capacity.

## 1. INTRODUCTION

The expanding range of tribological applications, habitually from industrial machinery to microscopic applications recently, has revived the importance and interest in this field. The hydrodynamic bearings are frequently used in wide range of applications and mechanisms since long. Many studies were dedicated to the study of the random influence roughness on the hydrodynamic journal bearing performance; the conclusion was that the roughness influences the bearing performance. The random roughness in hydrodynamic bearings may be introduced due to the presence of dust, additives in the lubricant and wear while the roughness may be random or deterministic nature. Surface texturing is claiming progressively more attention and is expected to be an important component in future bearing structure design. The presence of micrometer scale textures on a surface can modify the friction characteristics of that surface. It has long been known that micrometer-scale surface irregularities affect the load capacity of parallel sliding surfaces; however only recently have such textures been engineered to improve friction performance of mechanical parts micro textures act as micro-hydrodynamic bearings, enhancing load support and increasing film thickness, which leads to lower friction compared to untextured surfaces.

These studies highlighted the importance of dimple depth and its impact on reducing the friction coefficient. Other researches have shown that micrometer-scale roughness orientation plays a key role in friction characteristics. The packing density of the textures also affects friction. Fig 1 shows a schematic sketch of such surfaces interacting with a force F and a velocity u. To be able to separate these surfaces an internal force as big as F has to be developed in the opposite direction. This could be achieved by applying a pressure to a fluid between the surfaces. The force is then calculated as the pressure integral across the surface area. The pressure can be manually applied, which is called hydrostatic lubrication, or by letting kinematic energy from the walls be converted into fluid pressure, which is the concept of hydrodynamic lubrication.

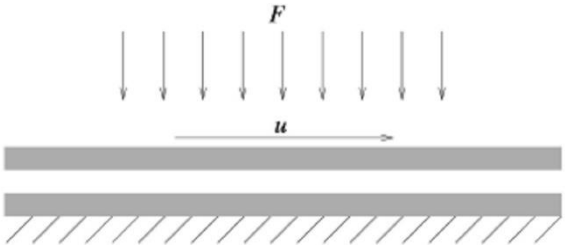


**Fig 1** Schematic sketch of surfaces interacting with a force F and a velocity u.

The greatest hydrodynamic pressure build-up is achieved by letting the surfaces form a small angle between them producing a geometric convergence. With some kind of fluid in between, the velocity u, on the wall will start driving fluid into the gap leading to a pressure build-up. Due to friction in the fluid film, the temperature will rise

www.ijprems.com
editor@ijprems.com

INTERNATIONAL JOURNAL OF PROGRESSIVE RESEARCH IN ENGINEERING MANAGEMENT AND SCIENCE (IJPREMS)

Vol. 02, Issue 09, September 2022, pp : 01-25

e-ISSN : 2583-1062

Impact Factor : 2.265

leading to thermal expansion of the fluid which in turn might produce a pressure rise as well. Examples of applications where this theory is applied are thrust and journal bearings where the fluid used is either a liquid or a gas.

## 2. HYDRODYNAMIC LUBRICATED BEARINGS

In these bearings the load-carrying surfaces are separated by a stable thick film of lubricant that prevents the metal-to-metal contact. The film pressure generated by the moving surfaces that force the lubricant through a wedge shaped zone. At sufficiently high speed the pressure developed around the journal sustains the load. The figure gives the exact description of a hydrodynamic journal bearing.

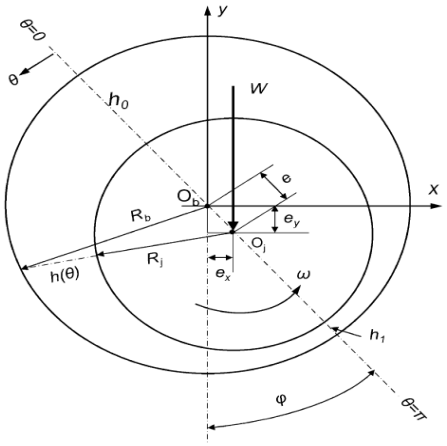


**Fig.2** Schematic Diagram of Journal bearing assembly

Here, Fig 2 shows the schematic diagram of journal bearing assembly. The hydrodynamic journal bearing in figure has a eccentricity of 'e' carrying a load W.

**Surface Texture**

Surface texture, also known as surface finish or surface topography, is the nature of a surface as defined by the 3 characteristics of lay, surface roughness, and waviness. It comprises the small local deviations of a surface from the perfectly flat ideal (a true plane).The term ‘surface texture’ refers to fine irregularities (peak and valley) produces on surface by forming process.

Surface texture is one of the important factors that control friction and transfer layer formation during sliding. Considerable efforts have been made to study the influence of surface texture on friction and wear during sliding conditions. Surface textures can be isotropic or anisotropic. Sometimes, stick-slip friction phenomena can be observed during sliding depending on surface texture.

**Lay:** Lay is the direction of the predominant surface pattern ordinarily determined by the production method used.

**Surface roughness:** Surface roughness commonly shortened to roughness, is a measure of the finely spaced surface irregularities. Surface roughness, is a component of surface texture. It is quantified by the deviations in the direction of the normal vector of a real surface from its ideal form. If these deviations are large, the surface is rough; if they are small, the surface is smooth. Roughness is typically considered to be the high-frequency, short-wavelength component of a measured surface.

Roughness plays an important role in determining how a real object will interact with its environment. Rough surfaces usually wear more quickly and have higher friction coefficients than smooth surfaces. Roughness is often a good predictor of the performance of a mechanical component, since irregularities in the surface may form nucleation sites for cracks or corrosion. On the other hand, roughness may promote adhesion.

**Waviness:** Waviness is the measurement of the more widely spaced component of surface texture. It is a broader view of roughness because it is more strictly defined as "the irregularities whose spacing is greater than the roughness sampling length". It can occur from machine or work deflections, chatter, residual stress, vibrations, or heat treatment. Waviness should also be distinguished from flatness, both by its shorter spacing and its characteristic of being typically periodic in nature.

**Use of Surface Texture on the Bearing Surface**

In the present work surface texture is used to study the influence of textures location on the bearing surface. The surface analysis, used in hydrodynamic lubrication, requires detailed statements of surface; a grid refined of this

www.ijprems.com
editor@ijprems.com

INTERNATIONAL JOURNAL OF PROGRESSIVE RESEARCH IN ENGINEERING MANAGEMENT AND SCIENCE (IJPREMS)

Vol. 02, Issue 09, September 2022, pp : 01-25

e-ISSN : 2583-1062

Impact Factor : 2.265

one and an important computing power. A numerical approach is used in order to give a description of the textures location effect on the most important characteristics in a hydrodynamic bearing. Through a wise choice of the textures arrangement on one of the bearing surfaces, its performance can be improved. The bearing surface is textured with cylindrical dimples.

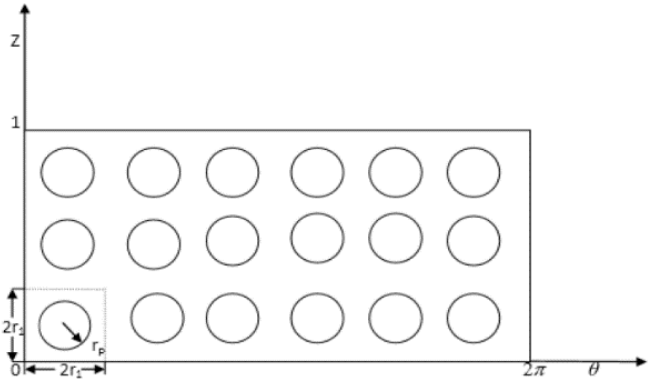


**Fig 3** Front view of cylindrical textured surface

Fig 3 shows cylindrical textures having a radius of $r_p$, having a grid size of $2r_1$ along θ-axis and $2r_2$ along Z-axis.

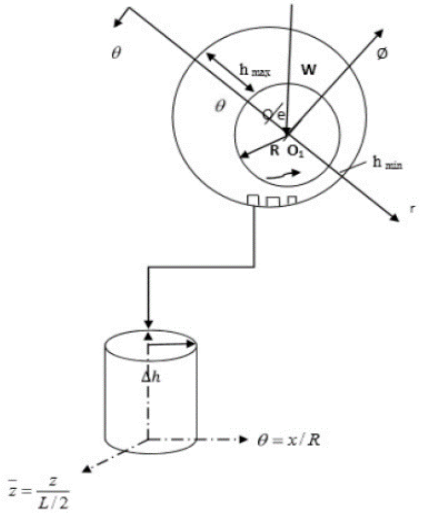


**Fig 4** Enlarged view of cylindrical texture

Fig 4 shows the enlarged view of the cylindrical texture having a height of Δh and where $h_{max}$ is the maximum distance of the centre of the shaft to the bearing.

## 3. VARIOUS IMPORTANT PARAMETERS USED IN BEARING DESIGN

**Length-to-diameter ratio:** The length to diameter ratio (l/d) affects the performance of the bearing. As the ratio increases, the resulting film thickness increases. A long bearing (l/d>1) therefore, has a more load capacity compared to short bearing (l/d<1). A short bearing, on the other hand, has greater side flow, which improves heat dissipation. The long bearing are more susceptible to metal to metal contact at two edges, when the shaft is deflected under load. Longer the bearing, the more difficult it to get sufficient oil flow through the passage between the journal and bearing. Therefore, the design trend is to use (l/d) ratio as 1 (i.e. square bearing) or less than 1.

**Unit bearing pressure:** The unit bearing pressure is the load per unit of projected area of the bearing in running condition. It depends upon a number of factors, such as bearing material, operating temperature, the nature and frequency of load and service conditions.

**Start-up Load:** The start-up load is the static load when the shaft is stationary. It mainly consist of the dead weight of shaft and its attachments. The start-up load can be used to determine the minimum length of the bearing on the basis of starting conditions. The unit bearing pressure for starting condition should not exceed 2 $N/mm^2$.

**Radial clearance:** The radial clearance should be small to provide the necessary velocity gradient. However, this requires costly finishing operations, rigid mountings of the bearing assembly and clean lubricating oil without any

INTERNATIONAL JOURNAL OF PROGRESSIVE RESEARCH IN ENGINEERING MANAGEMENT AND SCIENCE (IJPREMS)

www.ijprems.com
editor@ijprems.com

Vol. 02, Issue 09, September 2022, pp : 01-25

e-ISSN : 2583-1062

Impact Factor : 2.265

foreign particles. This increases the initial maintenance costs. The practical value of radial clearance is 0.001mm per mm of the journal radius.

**Minimum oil film thickness:** The surface finish of the journal and bearing is governed by the value of minimum oil film thickness selected by the designer and vice versa. There is a lower limit for the minimum oil thickness, below which metal to metal occurs and hydrodynamics film breaks.

**Maximum oil film temperature:** The lubricating oil tends to oxidize when the operating temperature exceeds $120^0$. Also the surface of Babbitt bearing tends to soften at $125^0$C (for bearing pressure 7N/mm$^2$) and at $190^0$C (for bearing pressure of 1.4N/mm$^2$). Therefore the operating temperature should be kept within these limits.

**Eccentricity:** The difference between center of bearing and centre of journal is called eccentricity and is denoted by 'e'

**Approach Used To Find Different Parameters of Textured Bearing**

Here 2 different approaches are used to find the required parameters

- Numerical approach using MATLAB
- ANSYS Fluent analysis.

## 4. NUMERICAL APPROACH USING MATLAB

During tribology studies physical values are often presented as differential equations that describe the laws of physics. These equations can be solved analytically but due to the fact that there may be many of them; they can be complicated and numerical methods which give approximate required solution are used. Appropriate software allows to obtain numerical solutions of equations representing mathematically formulated engineering problems. The basic methods of calculation used in

Computer programs The governing equation is the Reynolds equation in two dimensions. It can be written for an incompressible inviscid fluid as follows:

$$\frac{\partial}{\partial x}\left(\frac{\rho h^3}{\eta}\frac{\partial p}{\partial x}\right)+\frac{\partial}{\partial z}\left(\frac{\rho h^3}{\eta}\frac{\partial p}{\partial z}\right)=6U\frac{\partial}{\partial x}(\rho h)+12\frac{\partial}{\partial t}(\rho h) \quad (1)$$

Film thickness, $h = C + eCos\theta$ (1a)

$$\frac{\partial}{\partial \theta}\left(\bar{h}^{\,3}\frac{\partial p}{\partial \theta}\right)+\left(\frac{D}{L}\right)^2\frac{\partial}{\partial \bar{z}}\left(\bar{h}^{\,3}\frac{\partial p}{\partial \bar{z}}\right)=\frac{\partial \bar{h}}{\partial \theta}+2\lambda\frac{\partial \bar{h}}{\partial \tau} \quad (2)$$

Where, $\theta=\frac{x}{R},\bar{z}=\frac{z}{L/2},\bar{h}=\frac{h}{C},\bar{p}=\frac{pC^2}{6\eta UR},\tau=\omega_p t,\lambda=\frac{\omega_p}{\omega}$

Steady state Reynolds Equation can be written in dimensionless form as:

$$\frac{\partial}{\partial \bar{x}}\left(\bar{h}^3\frac{\partial \bar{p}}{\partial \bar{x}}\right)+\left(\frac{D}{L}\right)^2\frac{\partial}{\partial \bar{z}}\left(\bar{h}^3\frac{\partial \bar{p}}{\partial \bar{z}}\right)=3\frac{\partial \bar{h}}{\partial \bar{x}} \quad (3)$$

Where

$$\theta=\frac{x}{R},\bar{z}=\frac{z}{L},\bar{h}=\frac{h}{2C},\bar{p}=\frac{pC^2}{\eta\omega R^2}$$

Where

$\bar{x},\bar{z}$ - are non-dimensional hydrodynamic film co-ordinates [m],

L - is the bearing axial length [m],

d -diameter of the journal [m],

$\bar{p}$ - is the non-dimensional pressure,

$\bar{h}$ - is the non-dimensional hydrodynamic film thickness,

c -is the bearing radial clearance [m],

η -is the dynamic viscosity of the bearing [Pas],

ω –angular velocity [rad/s],

U = ω * d / 2

INTERNATIONAL JOURNAL OF PROGRESSIVE RESEARCH IN ENGINEERING MANAGEMENT AND SCIENCE (IJPREMS)

www.ijprems.com
editor@ijprems.com

Vol. 02, Issue 09, September 2022, pp : 01-25

e-ISSN : 2583-1062

Impact Factor : 2.265

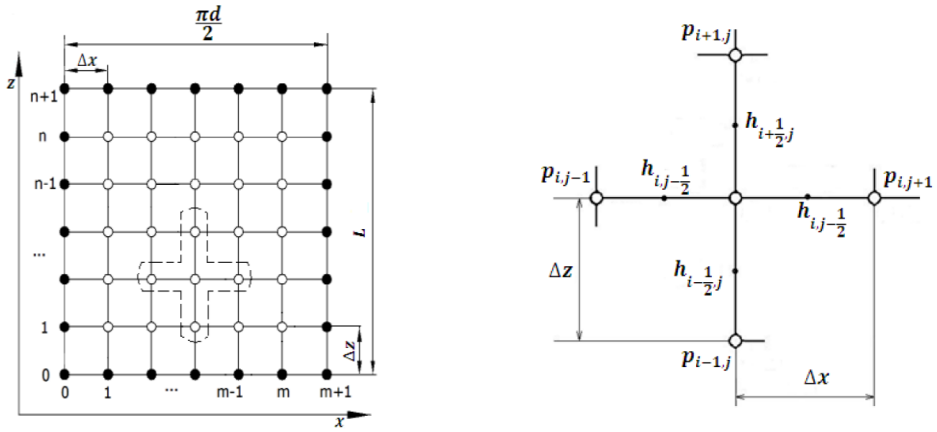


**Fig 5** FDM analysis of Non dimensional Reynolds Equations

Fig 5 shows separation of the set of nodal points for the finite difference method from the surface of the bearing a) schematic drawing showing the grid points used and b) view of a single set of five adjacent points.

In the point with the index's i, j (Fig 5) individual units of the Reynolds equation are brought closer, replacing the derivatives into differential quotients:

$$\frac{\partial}{\partial \bar{x}}(\bar{h}^3\frac{\partial \bar{p}}{\partial \bar{x}}) = \frac{h^3_{i,j+1/2}(\frac{\bar{p}_{i,j+1}-\bar{p}_{i,j}}{\Delta x}) - \bar{h}^3_{i,j-1/2}(\frac{\bar{p}_{i,j}-\bar{p}_{i,j-1}}{\Delta x})}{\Delta x} \quad (5)$$

$$\frac{\partial}{\partial \bar{z}}(\bar{h}^3\frac{\partial \bar{p}}{\partial \bar{z}}) = \frac{\bar{h}^3_{i,j+1/2}(\frac{\bar{p}_{i,j+1}-\bar{p}_{i,j}}{\Delta z}) - \bar{h}^3_{i,j-1/2}(\frac{\bar{p}_{i,j}-\bar{p}_{i,j-1}}{\Delta z})}{\Delta z} \quad (6)$$

$$\frac{\partial \bar{h}}{\partial \bar{x}} = \frac{\bar{h}_{i,j+1/2}-\bar{h}_{i,j-1/2}}{\Delta x} \quad (7)$$

After the substitution into (7) the difference quotients (6) and organizing them, the following expression about $\bar{p}_{i,j}$ is obtained:

$$\bar{p}_{i,j} = \frac{3\left(\frac{\bar{h}_{i,j-1/2}-\bar{h}_{i,j+1/2}}{\Delta \bar{x}}\right)+\left(\frac{d}{L}\right)^2\left(\frac{\bar{h}^3_{i-1/2,j}\bar{p}_{i-1,j}+\bar{h}^3_{i+1/2,j}\bar{p}_{i+1,j}}{\Delta \bar{z}^2}\right)+\left(\frac{\bar{h}^3_{i,j-1/2},\bar{p}_{i,j-1}+\bar{h}^3_{i,j+1/2},\bar{p}_{i,j+1}}{\Delta \bar{x}^2}\right)}{\left(\frac{\bar{h}^3_{i,j+1/2}-\bar{h}^3_{i,j-1/2}}{\Delta \bar{x}^2}+\left(\frac{d}{L}\right)^2\frac{\bar{h}^3_{i+1/2,j}-\bar{h}^3_{i-1/2,j}}{\Delta \bar{z}^2}\right)} \quad (8)$$

Equation (1.5) can be presented in general form:

$$\bar{p}_{i,j} = a_0 + a_1.\bar{p}_{i+1,j} + a_2.\bar{p}_{i-1,j} + a_3.\bar{p}_{i,j+1} + a_4.\bar{p}_{i,j-1} \quad (9)$$

Where $a_0, a_1, a_2, a_3, a_4$ are constant data for each grid point.

Pressure $\bar{p}_{i,j}$ is a function of these constants and a function of the four nearby pressure data (in the grid). For n*m grid points (Fig 1.6) n*m equations were obtained and further fixed in a program written in MATLAB environment. Finally, the way of pressure distribution p = p (x, z) was obtained. For points lying on the edge of the acetabulum there is no need to write the equation, since the pressure at these points is known.

If the pivot axis and the acetabulum are parallel, the thickness of the oil gap h is only a function of one variable angle φ:

$$h(\varphi) = \sqrt{\left(\frac{D}{2}\right)^2 + eD\sin(\alpha+\varphi) + e^2 - r} \quad (10)$$

The variable x is a linear function of radius D / 2 of the form:

$$x = \varphi.\frac{D}{2} \quad (11)$$

INTERNATIONAL JOURNAL OF PROGRESSIVE RESEARCH IN ENGINEERING MANAGEMENT AND SCIENCE (IJPREMS)

www.ijprems.com
editor@ijprems.com

Vol. 02, Issue 09, September 2022, pp : 01-25

e-ISSN : 2583-1062

Impact Factor : 2.265

Following transformation of derivative of h with respect to x is given by:

$$\frac{dh}{dx} = \frac{eD\cos(\alpha+\varphi)}{2\sqrt{\left(\frac{D}{2}\right)^2 + eD\sin(\alpha+\varphi) + e^2 - r}} \quad (12)$$

As before, at the point with the indexes i, j (Fig 1.6), with respect of the above formulas each word of the Reynolds equation (1.3) are brought closer by replacing pressure derivatives into differential quotients:

$$\frac{\partial}{\partial\bar{x}}(\bar{h}^3\frac{\partial\bar{p}}{\partial\bar{x}}) = 3\bar{h}^2\frac{d\bar{h}}{d\bar{x}}\frac{\partial\bar{p}}{\partial\bar{x}} + \bar{h}^3\frac{\partial^2\bar{p}}{\partial\bar{x}^2} = 3h_j^2\frac{d\bar{h}_j}{d\bar{x}}(\frac{\bar{p}_{i,j+1-}\bar{p}_{i,j-1}}{2\Delta\bar{x}}) + \bar{h}_j^3(\frac{\bar{p}_{i,j-1} - 2\bar{p}_{i,j} + \bar{p}_{i,j+1}}{\Delta\bar{x}^2})$$

$$\frac{\partial}{\partial\bar{z}}(\bar{h}^3\frac{\partial\bar{p}}{\partial\bar{z}}) = \bar{h}_j^{\,3}\frac{\partial^2\bar{p}}{\partial\bar{z}^2} = \bar{h}_j^3(\frac{\bar{p}_{i,j-1} - 2\bar{p}_{i,j} + \bar{p}_{i+1,j}}{\Delta\bar{z}^2}) \quad (13)$$

After the substitution and organizing them, the equation was obtained:

$$\frac{\partial}{\partial\bar{x}}(\bar{h}^3\frac{\partial\bar{p}}{\partial\bar{x}}) = 3\bar{h}^2\frac{d\bar{h}}{d\bar{x}}\frac{\partial\bar{p}}{\partial\bar{x}} + \bar{h}^3\frac{\partial^2\bar{p}}{\partial\bar{x}^2} = 3h_j^2\frac{d\bar{h}_j}{d\bar{x}}(\frac{\bar{p}_{i,j+1-}\bar{p}_{i,j-1}}{2\Delta\bar{x}}) + \bar{h}_j^3(\frac{\bar{p}_{i,j-1} - 2\bar{p}_{i,j} + \bar{p}_{i,j+1}}{\Delta\bar{x}^2})$$

$$\frac{\partial}{\partial\bar{z}}(\bar{h}^3\frac{\partial\bar{p}}{\partial\bar{z}}) = \bar{h}_j^{\,3}\frac{\partial^2\bar{p}}{\partial\bar{z}^2} = \bar{h}_j^3(\frac{\bar{p}_{i,j-1} - 2\bar{p}_{i,j} + \bar{p}_{i+1,j}}{\Delta\bar{z}^2}) \quad (14)$$

Replacing the matrix of unknowns at elements of $\bar{p}_{i,j}$ (i = 1: n, j = 1: m) on a single column vector $\bar{p}$ of $\bar{p}_k$ elements given by:

$$k = (i-1)m + j \quad (15)$$

Equation (11) can be written as:

$$a_{k,k-1}\bar{p}_{k-1} + a_{k,k}.\bar{p}_k + a_{k+1,k}.\bar{p}_{k,k+1} + a_{k,k-m}.\bar{p}_{k,k-m} + a_{k,k+m}.\bar{p}_{k,k+m} = b_k \quad (16)$$

The coefficients $a_{k,k-1}, a_{k,k}, a_{k+1,k}, a_{k,k-m}, a_{k,k+m}$ are elements different from zero in the matrix A, the $b_k$ coefficient is the element of one-column vector B. As a result a system of linear equations are given in a form of:

$$A\bar{p} = B \quad (15)$$

with $\bar{p}$ unknowns.

By solving numerically set of equations (15) according to the formula:

$$\bar{p} = A^{-1}B$$

pressure values are obtained.

**1.5.4 Non-Dimensional Load Capacity**

The non-dimensional steady state load components are given by

$$\bar{W}_{X_0} = \int_{\theta_1}^{\theta_2}\int_0^1 \bar{p}_0\cos\theta\, d\theta\, d\bar{z} \quad (16)$$

$$\bar{W}_{Z_0} = \int_{\theta_1}^{\theta_2}\int_0^1 \bar{p}_0\sin\theta\, d\theta\, d\bar{z} \quad (17)$$

$$\bar{W}_0 = \sqrt{\bar{W}_{X_0}^{\,2} + \bar{W}_{Z_0}^{\,2}} \quad (18)$$

The flow coefficient in the dimensionless form is given:

$$\bar{q}_Z = \frac{1}{2}\left(\frac{D}{L}\right)^2\int_0^{2\pi}\bar{h}_0^{\,3}\frac{\partial\bar{p}_0}{\partial\bar{z}}d\theta \quad (19)$$

www.ijprems.com
editor@ijprems.com

INTERNATIONAL JOURNAL OF PROGRESSIVE RESEARCH IN ENGINEERING MANAGEMENT AND SCIENCE (IJPREMS)

Vol. 02, Issue 09, September 2022, pp : 01-25

e-ISSN : 2583-1062

Impact Factor : 2.265

The friction variable,

$\bar{\mu} = (R/C)\mu = \frac{\bar{F}}{\bar{W}_0}$ , is given:

$$\bar{\mu} = \mu(R/C) = \frac{\int_0^{2\pi} (3\bar{h}\frac{\partial \bar{p}_0}{\partial \theta} + \frac{1}{\bar{h}})d\theta}{6\bar{W}} \quad (20)$$

## 5. CFD ANALYSIS

CFD is an acronym for Computational Fluid Dynamics and involves solving fluid flow problems in a computational discrete iterative manner. The subject of solving fluid flows is often complicated and has earlier only been possible for simple cases where certain terms of the governing equations could be neglected in such a way that the problem could be solved analytically. Computational codes for solving structural mechanics problems have been around for a reasonably long time and are well established in the different research areas. CFD-codes are however a bit less established on the market, but have from some ten years ago up to now increased a lot in usage in the industrial and research community. This is mainly because of a tremendous increase in computer performance and at the same time a decrease in costs in the last years.

The basic governing equations for fluid flow include non-linear partial derivatives and can only be solved analytically for simple cases. One frequently used approximation to the governing equations of fluid flow is the Reynolds equation which is used in thin fluid films. In Reynolds equation the inertia term is neglected. This is usually a good approximation for fluid film lubrication with smooth walls. If, however, the walls marking off the thin fluid film contains some geometrical perturbations, the inertia term can significantly influence the flow and the Reynolds approximations are not obvious. It is therefore important to analyze if the simplifications are physically acceptable in each case in order to receive relevant solutions. In some cases the problems can only be solved numerically with a CFD-technique because of the complexity of the flow. In fluid mechanics the use of CFD is today well established, as compared to the tribology1 community, where the use of CFD has not been equally widespread. This might be explained by the type of flow applications which are most often thin fluid films, and the flow equations can be simplified accordingly. CFD has in the recent years however taken its first steps into the tribology community and is advancing continuously.

Fluid dynamics is a field of science which studies the physical laws governing the flow of fluids under various conditions. Great effort has gone into understanding the governing laws and the nature of fluids themselves, resulting in a complex yet theoretically strong field of research.

Computational Fluid Dynamics or CFD as it is popularly known, is used to generate flow simulations with the help of computers. CFD involves the solution of the governing laws of fluid dynamics numerically. The complex set of partial differential equations are solved on in geometrical domain divided into small volumes, commonly known as a mesh (or grid).

CFD has enabled us to understand the world in new ways. We can now see what it is like to be in a furnace, model how blood flows through our arteries and veins and even create virtual worlds. CFD enables analysts to simulate and understand fluid flows without the help of instruments for measuring various flow variables at desired locations.

## 6. LITERATURE REVIEW

Fluid film lubrication is an area which is subject to much research. This is due to the widespread range of applications which in turn leads to the fact that a small improvement in bearing performance can be substantially economically beneficial. The main area of this research is focused on hydrodynamic effects of a textured surface. This has been subject to both analytical and experimental research over the last few years and various results have been achieved on lubrication performance.

Snegovski and Bulyuket al.[1] conducted an experiment to study journal bearings with and without micro-grooves on the shaft. Parts of the shaft had surface micro-relief formed by a system of non-intersecting sinusoidal microgrooves obtained by the vibrating roll-forming method. According to the authors the load carrying capacity was increased 1.5-2 times compared to a smooth shaft for sliding velocities ranges from 30 to 60 m/s. For grooves greater than 12 - 15 μm no improvement in bearing performance was achieved. The same bearings were tested in the low speed range. Frictional losses were reduced by 10 to 15% with the dimpled shaft. Bulyuk worked on thermal analysis

of sliding bearings with micro-channels on the shaft. He claimed that there is a forced turbulization in the loaded zone. The heat removal from the shaft becomes 1.8 - 4 times greater with micro-channels compared with smooth shaft. The load capacity without grooves is decreased when the velocity increases. This is, according to the authors, due to inadequate heat transfer from the loaded zone. The reason for better load carrying capacity with micro-grooves is claimed to be due to additional lubrication and circulation through the loaded zone.

A similar statement is made by Bulyuk, where the research is focused on thermal analysis of sliding bearings with micro-channels on the shaft. Applying micro-channels leads to intermixing of the lubricant for certain velocities and effective fluid-film thickness. Bulyuk claims that there is a forced turbulization in the loaded zone. The heat removal from the shaft becomes 1.8–4.0 times greater with micro-channels than without.

In an experimental setup with pending pad bearing a reduction of the coefficient of friction by 7.3% is achieved with 16% groove area density on one surface compared to a plain surface. The authors suggest that further research should be focused on optimizing the size, shape, pattern and orientation of the grooves.

A theoretical approach to finding hydrodynamic effects of micro-grooves is made by Ronen and Etsionet al.[2] in where the focus lies on friction force. Reynolds equation, including an inertia term is solved with an iterative method. The application is a piston ring with applied micro-grooves. The interacting surfaces are thus completely parallel. The inertia parameter had little effect on the average friction force. The average friction force is reduced with increasing number of grooves.

An example, not of surface texturing, but of a computational approach in a similar regime is presented where the analysis is focused on the fore-region, i.e. the large pocket in front of the surfaces of a thrust bearing pad. A Computational Fluid Dynamics technique is used and the constant terms are temperature, viscosity and density. An optimal fluid film ratio $h_2/ h_1$ is achieved, where $h_1$ = inlet film thickness and $h_2$ = outlet film thickness. An interesting result is that the load capacity is increased by including fluid inertia in the calculations and by including fluid flow in the fore-region.

Previous research, which has mainly been experimental, has shown that textured surfaces in some cases lead to interesting hydrodynamic effects. With practical experiments, however, it may be hard to achieve good spatial resolution. The probes used in various measurements are not infinitesimally small and the level of noise in the measurements may be factors that limit the highest possible resolution. In order to understand the flow phenomena occurring in these small regimes to a higher degree, a computational approach is needed. With a computational approach, geometrical and physical variables are easily changed and results from different flow conditions can be achieved with low effort. One such approach could be Computational Fluid Dynamics.

Hamilton et al. [3] published one of the earliest works on the application of deterministic surface features in 1966. That research described a theory of liquid lubrication applicable to parallel surfaces of a rotary shaft face seal. The lubrication mechanism was based on surface micro-irregularities and associated film cavities. A theoretical model for deterministic micro asperities was presented. Three surface texture patterns were photoetched onto the stator surface and load capacities were found experimentally. The theoretical results agreed quantitatively with the experiments for these asperity distributions.

Anno et al. [4] published further research succeeding their previous work in 1966. In this work the theory of load support for micro asperity lubrication was further revised by hypothesizing small tilts on asperity tops. This hypothesis was attributed to the fact that for certain deterministic asperities, the authors found a huge difference between the theory and experimental results. Although direct evidence of the tilt hypothesis was lacking at that time, the authors demonstrated that the load support is even further increased when the tops of asperities are purposefully rounded and thus suggested the use of planned micro asperities as an effective method for lubricating the parallel faces of seals and thrust bearing surfaces.

Anno et al. [5] published further research on micro asperity lubricated face seals. In this work, theory and experimental work on the leakage of lubricant from micro asperity covered faces was reported. It was concluded that the leakage from micro asperity lubricated seals follows the predictions of Poiseuille flow, with the exception that a significant effect of rotor rotation is observed. However, significantly low leakage, typically of the order of 0.2 in3/hr for a channel height of 10-4 in and a pressure drop of 10 psi across the seal face, was recorded due to the micro asperity lubricated seal face.

Etsion and Burstein et al. [6] developed a mathematical model to allow performance prediction of all non-contacting mechanical seals having a regular micro-surface structure in the form of hemispherical pores. Seal performance such as equilibrium face separation, friction torque and leakage across the seal are calculated for a range

of seal pressures, pore sizes and pore ratio of the ring surface area. An optimum pore size was found that depends on other variables and corresponds to maximum axial stiffness and minimum friction torque.

Sinanoglu [7] is investigated the tribological performance of threaded texture shaft surfaces by experimental and theoretical neural network approaches. It is suggested that the screw thread act as a hydrodynamic bearing and micro-reservoir. The screw thread supplies the lubricant in starved lubricant condition. It has been found that the load-bearing capacity is substantially enhanced in a certain degree of threaded textured shaft surface than shaft surface without texture.

Rahmani et. al. [8] have performed the analytical study of slider bearing with textures surface. three shapes are considered in the study like rectangular, triangular rectangular, and isosceles triangular. It has been noted that the shape and type of texture can significantly affect the performance of the bearing [8]. Two parameters i.e., optimum height and textured area ratio are considered for the investigation. The optimisation has been performed to set the optimum texturing parameter for evaluating the maximum load capacity, minimum friction, and load capacity to lubricant flow rate [8].

Tala-Ighil et al. [9] examine the bearing characteristics for cylincrical textured journal bearing theoretically. The study analysed the bearing characteristic under three different conditions, partially textured full textured and deep textured. It has been observed that full texturing is ineffective and can not lift the shaft through the hydrodynamic effect due to the cavitation effect [9]. However, partially texture bearing can lift the shaft when texturing is done on the decline part of hydrodynamic pressure. Moreover, the deep texture gives the maximum,bearing performance at the eccentricity ratio of 0.6 when declined part of the pressure field is textured [9].

Cupillard et.al. [10] analysed the inertia effect of fluid on textured hydrodynamics contacts. In the analysis, textured depth is optimised and critical depth of textured is set, above the critical textured depth negative inertia effect is obtained below this critical textured depth positive inertia effect is noted. However, high load carrying capacity is found high at the optimum textured depth, which is relatively greater than the critical textured depth. It is also noted that above the optimum texture load carrying capacity decreases significantly due to the finding of the recirculation zone [10].

**S.** Kango et. al. [11] analysed the performance of micro texture journal bearing under the combined effect of heat dissipation and non-Newtonian rheological lubricant. The performance has been analysed using the mass conservation algorithm (JFO boundary condition) and found more realistic results in the JFO boundary condition than the Reynolds boundary condition.

Gupta et. al [12] analysed the textured hydrodynamic journal bearing, experimentally. The texture is prepared with help of a mechanical indentation technique on the inner side of the journal bearing surface and a large tribological data is captured for investigating the comparative analysis between smooth and textured journal bearing. the result of analysed data shows higher tribological for texture journal bearing [12].

Qui et. al. [13] analysed the textured parallel sliding surface lubricated with gaseous lubricants. Various textured shapes i.e., spherical, ellipsoidal, circular, elliptical, triangular, and chevron-shaped dimples are considered while analyzing the tribological performance of the bearing. The compressible Reynolds equation is solved to obtain the pressure distribution and load carrying capacity for the domain having ten dimples. Additionally, the geometry of

the textures and the texture density is optimised as a function of operating parameters i.e., relative velocity and space between the sliding surfaces. The ellipsoidal shape texture onthe sliding surface results in maximum load-carrying capacity [13].

Reddy and Kakoty [14] use the elliptical texture on the journal bearing surface to evaluate the

performance of the journal bearing. The analysis suggested a significant improvement in the tribological performance of the journal bearing with elliptical texture. The analysis reported an increase in flow co-efficient and reduction in friction variables [14].

Malik and Kakoty [15] investigated the performance of parallel and inclined slider bearings in which the surface of the slider bearing has been constructed with the dimpled texture. The simple non-dimensional technique is used in the analysis, and the textured directionality effect has been taken into consideration. The improvement in bearing performance is noted in the forward texturing, and on the contrary, lower bearing performance is indicated in backward texturing [15].

www.ijprems.com
editor@ijprems.com

INTERNATIONAL JOURNAL OF PROGRESSIVE RESEARCH IN ENGINEERING MANAGEMENT AND SCIENCE (IJPREMS)

Vol. 02, Issue 09, September 2022, pp : 01-25

e-ISSN : 2583-1062

Impact Factor : 2.265

## 7. ANALYSIS USING ANSYS AND MATLAB

**CFD Analysis**

ANSYS Fluent solves the geometries using the finite volume method. Navier-stokes equation is solved for the conservation of energy, conservation of momentum and the continuity equation. Important settings are as follows:

1. Flow is supposed to be laminar and hence laminar model is chosen for the simulation.
2. The effect of gravity has been taken into picture.
3. Pressure based and steady state implicit solver is chosen for the simulation.
4. Pressure outlet is at the zero gauge pressure.
5. The fluid inlet velocity is 25m/s in all the geometries.
6. SIMPLE scheme is chosen for solving the problem.

The geometry is modelled using the Modular Design workbench of the ANSYS software. The geometry is chosen based on the wedge shape obtain in the hydrodynamic journal bearing between the journal and the bearing surface. The lubricant enters from the top right region (as shown in fig 6) and exits from the top left region. The figure shows the cross sectional view of the bearing along with the lubricant flow path.

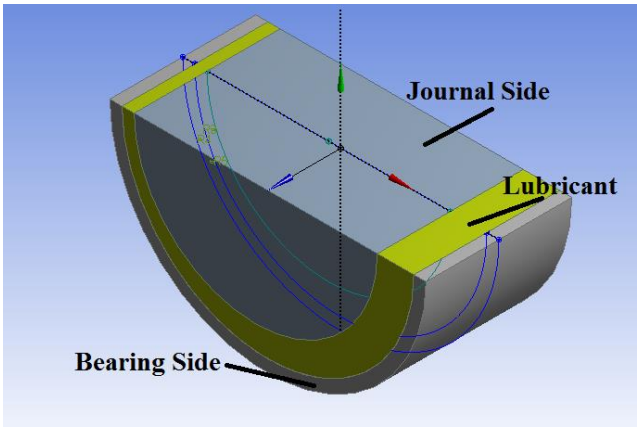


**Fig 6** Cross Sectional view of bearing

CFD simulations are performed with the help of four different geometries. The geometries are as follows:

a. Geometry with no type of texturing (Fig 6)
b. Geometry with a rectangular shaped (type R-1) texturing along the bearing plate
c. Geometry with a rectangular shaped (type R-2) texturing along the bearing plate
d. Geometry with prism shaped (type T-1) texturing along the bearing plate
e. Geometry with prism shaped (type T-2) texture on the bearing surface and rectangular shaped (type R-3) texturing along the journal boundary.

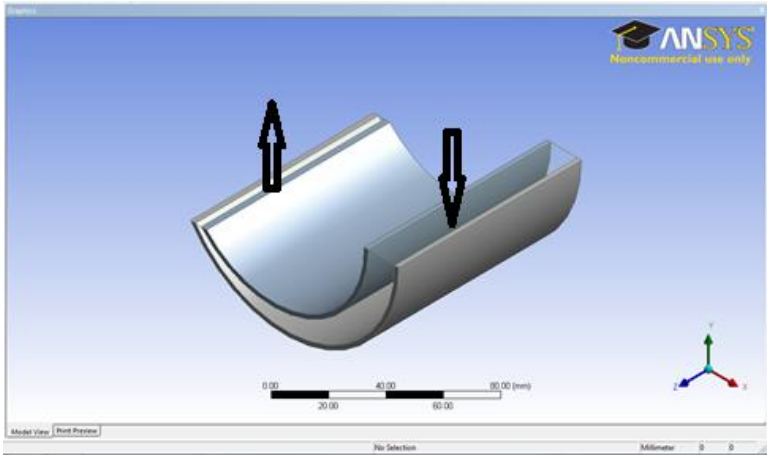


**Fig 7** Geometry with no type of texturing

Fig 7 has no texture etched on the surface. The inlet and outlet directions of the lubricant are also shown in the figure.

INTERNATIONAL JOURNAL OF PROGRESSIVE RESEARCH IN ENGINEERING MANAGEMENT AND SCIENCE (IJPREMS)

www.ijprems.com
editor@ijprems.com

Vol. 02, Issue 09, September 2022, pp : 01-25

e-ISSN : 2583-1062

Impact Factor : 2.265

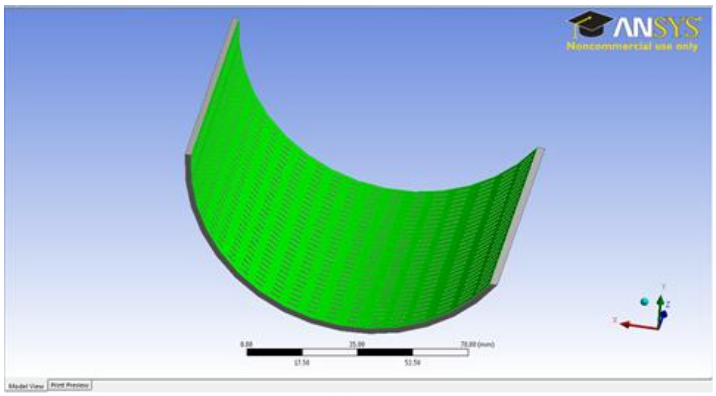

**Fig 8** Geometry with a rectangular shaped texture

The geometry of the surface of the bearing (Fig 8) is etched with rectangular grooving along the bearing surface.

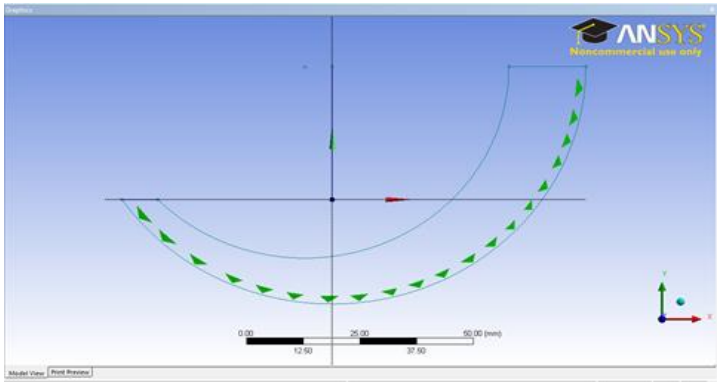

**Fig 9** Geometry with a prismatic shaped texture

The prismatic geometry is also chosen for analysis as shown in Fig 9 The texturing is done along the bearing surface.

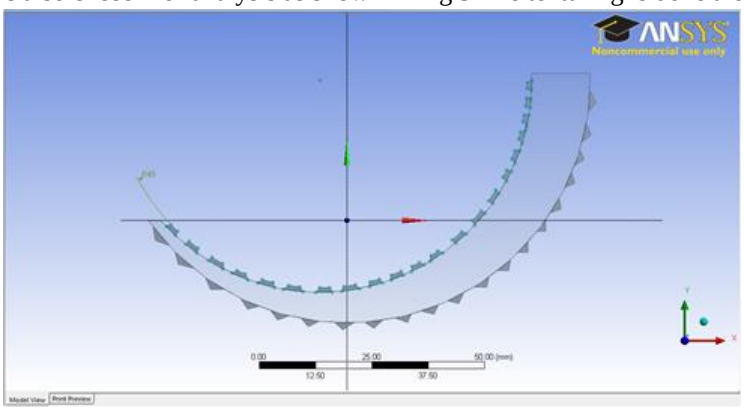

**Fig 10** Geometry with prism shaped and rectangular shaped texture

The journal geometry is also textured here with rectangular shaped textures along with prismatic textures on the bearing surface as shown in Fig10

**Named selections**

The geometry is named accordingly to make the simulation easily. It is shown in Fig 11.

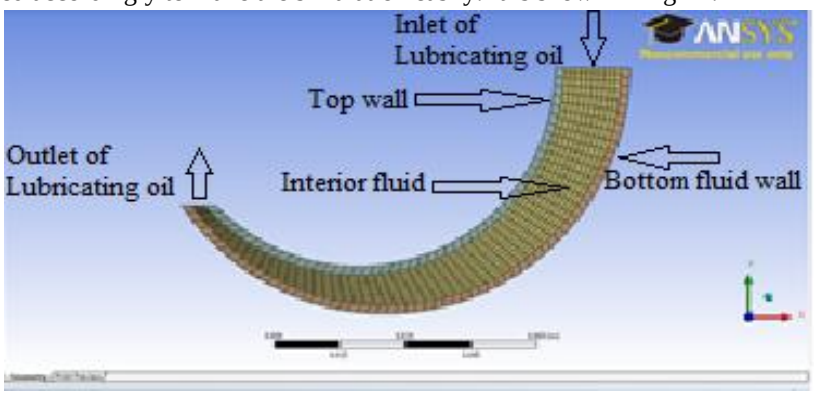


**Fig 11** Named selections

www.ijprems.com
editor@ijprems.com

INTERNATIONAL JOURNAL OF PROGRESSIVE RESEARCH IN ENGINEERING MANAGEMENT AND SCIENCE (IJPREMS)

Vol. 02, Issue 09, September 2022, pp : 01-25

e-ISSN : 2583-1062

Impact Factor : 2.265

Fluid_Region, Velocity_Inlet, Pressure_Outlet, Fluid_side_wall, Top_wall_fluid, Fluid_bottom_texture_side are the different named sections that are used in our analysis.

**Description of dimensions:**

Length of the bearing, L = 45 mm

Diameter of the bearing, D = 108 mm

Diameter of the journal, d = 90 mm

L/d ratio = 1/2

Radial clearance, c= R-r = 9 mm

Eccentricity, e = 6 mm

Eccentricity ratio, ε = e/c = 0.67

Number of Nodes = 15399, Number of Elements = 62577 (for the non-textured geometry)

Aluminum is used as a material for bearing and journal and Benzene is used as lubricating oil in our case. The properties are chosen as default as in ANSYS Fluent software.

**3.1.3 Specifications of the different types of textures:**

1. Rectangular grooving with 0.5 mm depth (R-1 type)
2. Rectangular grooving with 1.0 mm depth (R-2 type)
3. Prismatic grooving with 1.5 mm depth (T-1 type)
4. Prismatic grooving with 1.5 mm depth (T-2 type) and rectangular grooving with 1mm depth (R-3type)

## 8. NUMERICAL ANALYSIS USING MATLAB

In the numerical analysis, we have used Reynolds equation in non-dimensional form for hydrodynamic journal bearings. The journal bearing is a type of a fluid bearing which is designed for carrying radial loads.

Equation (8) is solved using a finite difference numerical scheme. The finite difference equation is solved using Gauss-Seidel method with square staggered grids. The different running conditions and different parameters are used for obtaining the favourable output conditions.

**Gauss-Seidel Method**

The Gauss–Seidel method is an iterative technique for solving a square system of n linear equations with unknown $x$ :

$$Ax = B \tag{21}$$

It is defined by the iteration

$$L_* x^{k+1} = b - U x^{(k)} \tag{22}$$

Where $x^{(k)}$ is the kth approximation or iteration of $x$, $x^{k+1}$ is the next or k + 1 iteration of $x$, and the matrix A is decomposed into a lower triangular component $L_*$ and a strictly upper triangular component U

$$A = L_* + U \tag{23}$$

In more detail, write out A, $x$ and $b$ in their components:

$$A = \begin{bmatrix} a_{11} & a_{12} & \cdot & a_{1n} \\ a_{12} & a_{22} & \cdot & a_{2n} \\ \cdot & \cdot & \cdot & \cdot \\ a_{1n} & \cdot & \cdot & a_{nn} \end{bmatrix} \quad X = \begin{bmatrix} x_1 \\ x_2 \\ \cdot \\ x_n \end{bmatrix} \quad B = \begin{bmatrix} b_1 \\ b_2 \\ \cdot \\ b_n \end{bmatrix} \tag{24}$$

Then the decomposition of A into its lower triangular component and its strictly upper triangular component is given by:

$$A = L_* + U \tag{25}$$

$$L_* = \begin{bmatrix} a_{11} & 0 & \cdot & \cdot & 0 \\ a_{12} & a_{22} & \cdot & \cdot & 0 \\ \cdot & \cdot & \cdot & \cdot & \cdot \\ \cdot & \cdot & \cdot & \cdot & \cdot \\ a_{1n} & a_{2n} & \cdot & \cdot & a_{nn} \end{bmatrix} \quad U = \begin{bmatrix} 0 & a_{12} & \cdot & \cdot & a_{1n} \\ 0 & 0 & \cdot & \cdot & a_{2n} \\ \cdot & \cdot & \cdot & \cdot & \cdot \\ \cdot & \cdot & \cdot & \cdot & \cdot \\ 0 & 0 & \cdot & \cdot & 0 \end{bmatrix} \tag{26}$$

www.ijprems.com
editor@ijprems.com

INTERNATIONAL JOURNAL OF PROGRESSIVE RESEARCH IN ENGINEERING MANAGEMENT AND SCIENCE (IJPREMS)

Vol. 02, Issue 09, September 2022, pp : 01-25

e-ISSN : 2583-1062

Impact Factor : 2.265

The system of linear equations may be rewritten as:

$$L_* x = b - Ux \tag{27}$$

The Gauss–Seidel method now solves the left hand side of this expression for $x$, using previous value for $x$ on the right hand side. Analytically, this may be written as:

$$x^{k+1} = L_*^{-1}\left(b - Ux^k\right) \tag{28}$$

However, by taking advantage of the triangular form of $L_*$, the elements of $x^{k+1}$ can be computed sequentially using forward substitution.

$$x_i^{k+1} = \frac{1}{a_{ii}}\left(b_i - \sum_{j<i} a_{ij} x_j^{(k+1)} - \sum_{j>i} a_{ij} x_j^{(k)}\right) \tag{29}$$

Where $i, j = 1, 2, ....., n$

The procedure is generally continued until the changes made by an iteration are below some tolerance, such as a sufficiently small residual.

## 9. MATLAB ALGORITHM

The logic behind the MATLAB code is finite difference method using Gauss-Seidel technique. An array of pressure was initialized with initial zero value and initial error was defined. The area fraction of the micro cavities was defined along with different depth of the cavities. The variable depths was selected to optimize for the best depth of the surface texture. An initial function accommodated all the different values included in the analysis. Iterations were permitted for errors included in the program. A while loop and for loop along with if-else logic was repeated. The geometry was defined using matrix. The cylindrical, triangular and rectangular geometry was defined in the geometry of the program. The mesh function meshed the geometry along the axes which included the cavities. The geometry angles were used extensively to relate the pressure with the input parameters. The boundary condition was imposed upon the structure to limit the function within the boundary limits. The load calculation code was formulated from the initial Reynolds equation and later defined in the geometry used in the code. The friction co-efficient was also defined for the parameters included in the geometry. Using the bearing characteristic parameters Sommerfeld number is also calculated. The Sommerfeld number is helpful to the designers, because it includes design parameters, bearing dimensions, friction, viscosity, speed of rotation and bearing pressure. But it does not include the bearing arc. Therefore the functional relationship can be obtained for bearings with different arcs. The basic objective of finding the load carrying capacity and friction co-efficient is to increase the efficiency of the bearing to transport motion between parts.

**MATLAB Geometries**

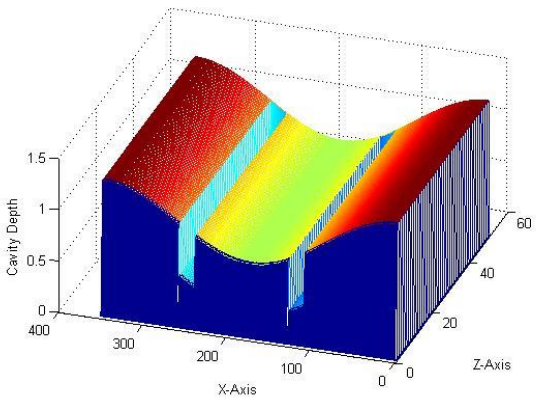


**Fig 12 ε** = 0.3, Rectangular shaped textures

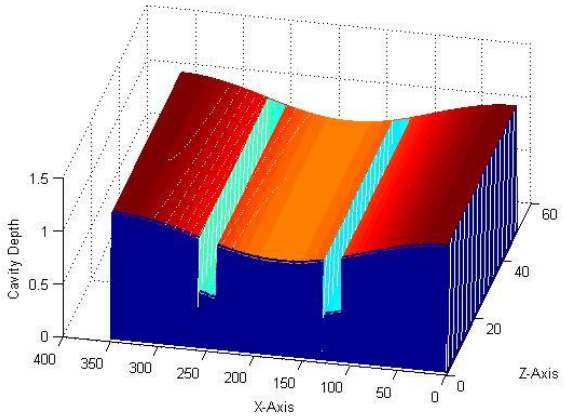


**Fig 13 ε** = 0.15, Rectangular shaped textures

The bearings with rectangular textures are shown in Fig 12 and Fig 13 for different eccentricities. The colour code show the different value of depths over the surface. The texture is along the z-axis.

INTERNATIONAL JOURNAL OF PROGRESSIVE RESEARCH IN ENGINEERING MANAGEMENT AND SCIENCE (IJPREMS)

www.ijprems.com
editor@ijprems.com

Vol. 02, Issue 09, September 2022, pp : 01-25

e-ISSN : 2583-1062

Impact Factor : 2.265

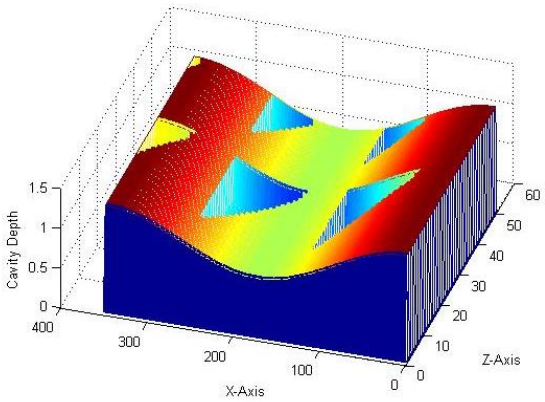


**Fig 14** $\varepsilon$ = 0.3, Triangular shaped textures

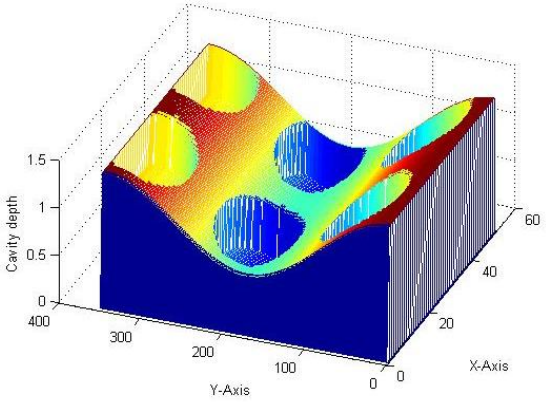


**Fig 15** $\varepsilon$ = 0.4, Cylindrical shaped texture

The bearings with triangular textures and cylindrical textures are shown in Fig 14 and Fig 15 for eccentricities 0.3 and 0.4 respectively. The colour code show the different value of depths over the surface. The texture is along the z-axis.

**Different Input Parameters used**

i. Length to diameter ratio=1
ii. Grid size along x-axis, P=400
iii. Grid size along y-axis, Q=100
iv. Individual grid size along x-axis=$2\pi/P$
v. Individual Grid size along y-axis=$1/Q$

## 10. RESULTS OBTAINED FROM CFD ANALYSIS

Results obtained through CFD simulations of the geometries namely a) smooth surface b) rectangular grooves on bearing c) prismatic grooves on bearing d) grooves on both sides with rectangular on journal and prismatic on bearing, are discussed in ANSYS Fluent workbench.

**Geometry with no type of texturing**

The results obtained for no textures are compared with the help of pressure & velocity contours and the pressure & velocity graphs across the fluid region and the bearing wall.

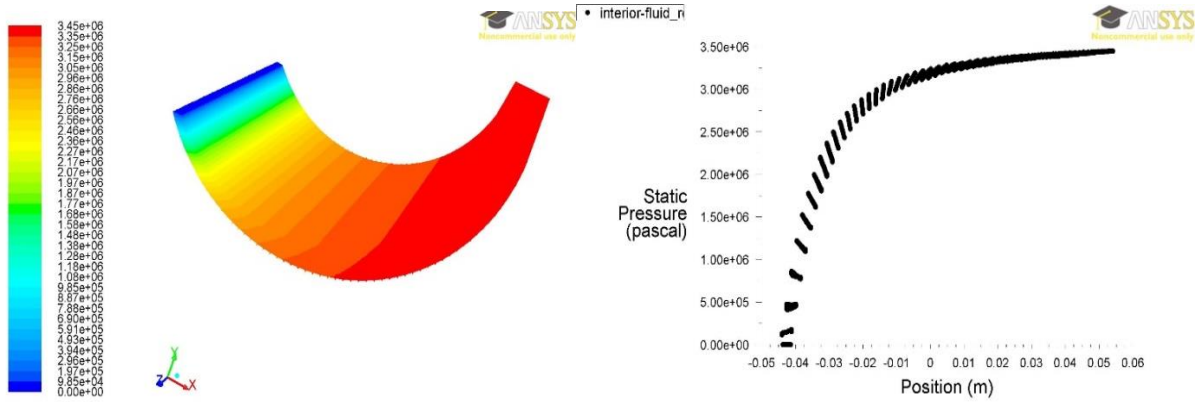


**Fig 16** Pressure variation in the flow region

Fig 16 show the variation of pressure along the flow direction from inlet to outlet. From inlet to outlet the area of cross-section replicates the wedge shape and hence the converging region. As the flow reaches the outlet, the pressure of the fluid region increases as shown in figures. This increase in the pressure supports the external load. In the non-texture geometry of present case, the maximum pressure of the fluid reaches to $3.45 \times 10^6$ Pa. The pressure increases gradually near the inlet section and it remains constant near the outlet section as shown in the figure.

INTERNATIONAL JOURNAL OF PROGRESSIVE RESEARCH IN ENGINEERING MANAGEMENT AND SCIENCE (IJPREMS)

www.ijprems.com
editor@ijprems.com

Vol. 02, Issue 09, September 2022, pp : 01-25

e-ISSN : 2583-1062

Impact Factor : 2.265

**Geometry with a rectangular shaped (type R-1) texturing along the bearing plate**

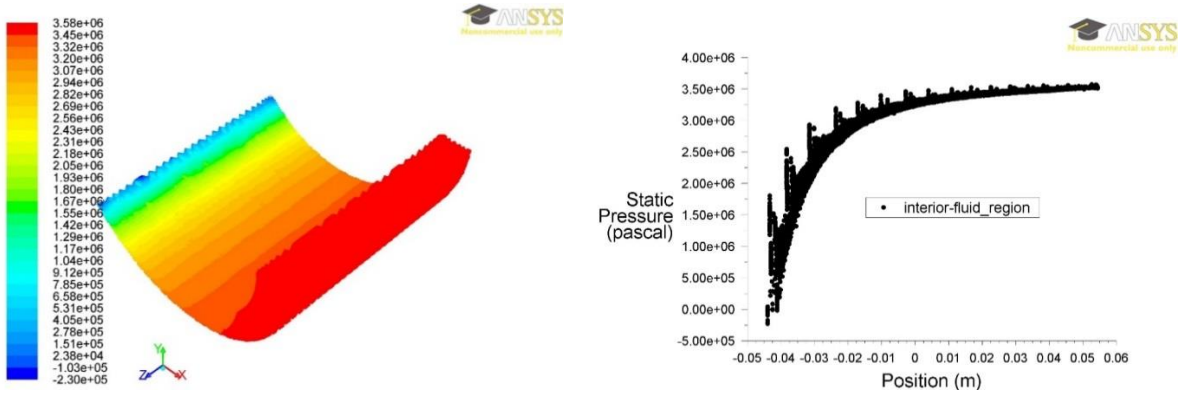


**Fig 17** Variation of Pressure in the flow region

Fig 17 show the results for the type R-1 geometry. From the plots of the pressure developed along the flow region and the bearing surface, it is inferred that, the pressure increases along the flow direction same as the non-textured geometry (Fig 17). However, there are sudden rise in the pressure of fluid due to the texturing. Hence the net sum of the pressure along the flow increases and thus increases the load carrying capacity of the bearing fluid.

**Geometry with a rectangular shaped (type R-2) texturing along the bearing plate**

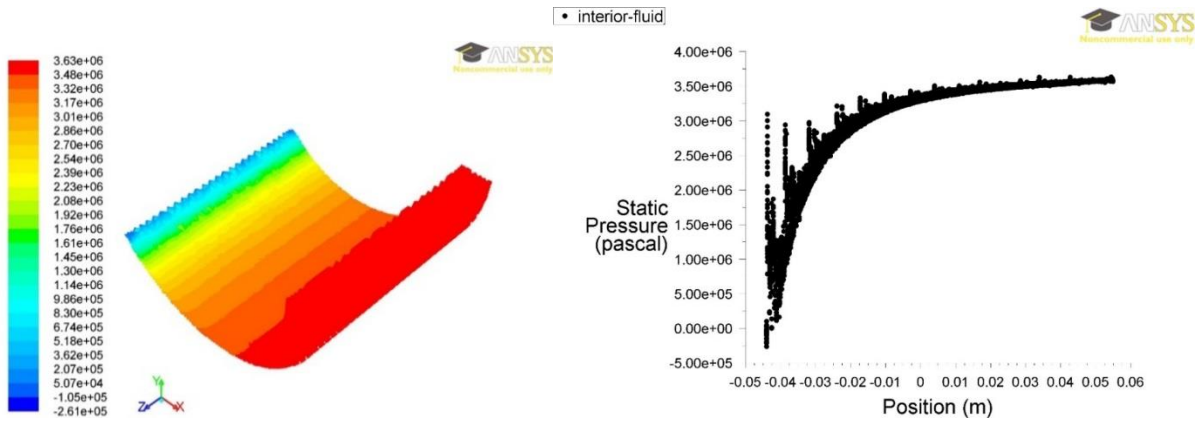


**Fig 18** Pressure variation in the flow region

Fig 18 show the result for the type R-2 texturing. In this case, the depth of the rectangular texture is decreased from 1mm (as in type R-1) to 0.5mm. This change in the dimension parameter, effects the pressure generation along the flow region as shown in the Fig 18. There is increased pressure due to the R-2 type of texturing. The maximum pressure in the fluid reaches up to 3.63x $10^5$ Pa which is more as compared to the previous geometries.

**Geometry with prism shaped (type T-1) texturing along the bearing plate**

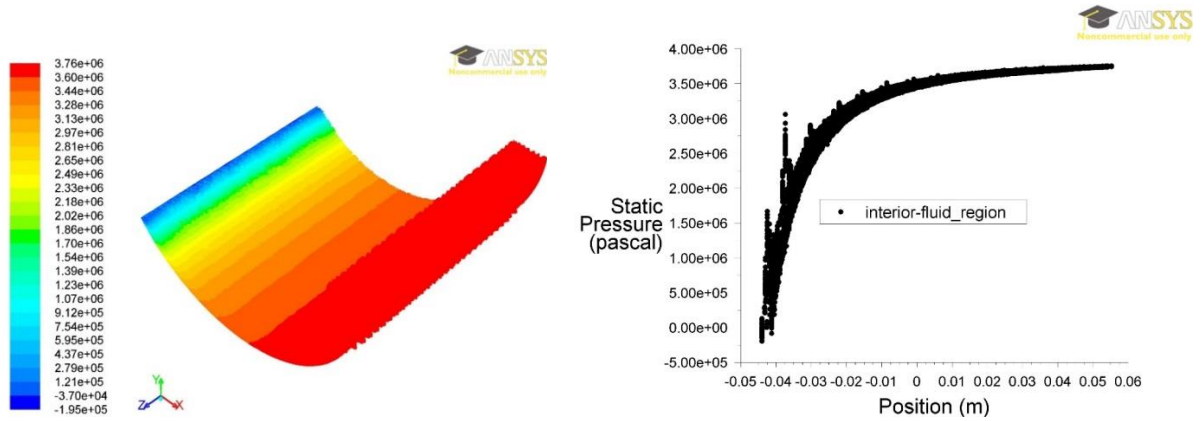


**Fig 19** Pressure variation in the flow region

In the same way, the effects of the type T-1 geometry is compared with the previous geometries. The results are shown in the Fig 19 Clearly, the texturing effects the load carrying capacity of the bearing.

www.ijprems.com
editor@ijprems.com

INTERNATIONAL JOURNAL OF PROGRESSIVE RESEARCH IN ENGINEERING MANAGEMENT AND SCIENCE (IJPREMS)

Vol. 02, Issue 09, September 2022, pp : 01-25

e-ISSN : 2583-1062

Impact Factor : 2.265

**Geometry with prism shaped (type T-2) texture on the bearing surface and rectangular shaped (type R-3) texturing along the journal boundary**

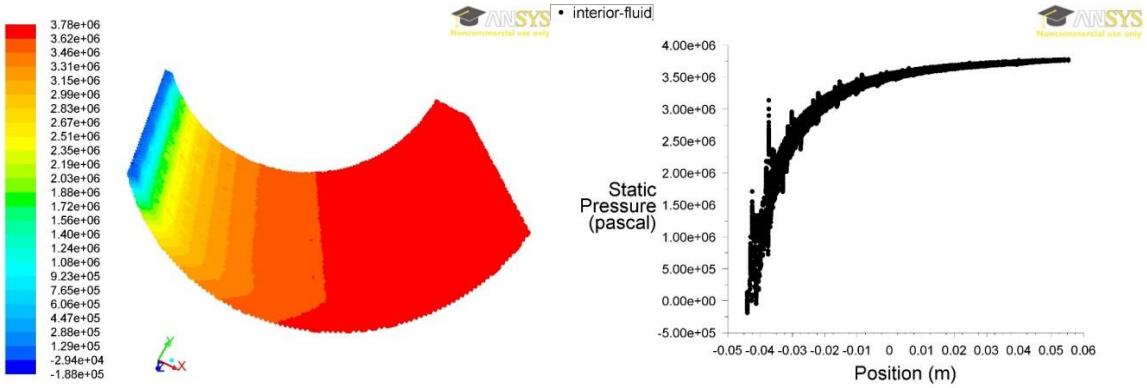


**Fig 20** Pressure variation in the flow region

Fig20 show the variation of pressure along the flow path and is increasing in the texturing region, which is more than that of the previous geometries.

The various values of maximum pressure in different geometries are tabled below:

**Table 1** Different values of pressure for different models

| Model | Maximum Pressure (in $10^6$ Pa) |
|---|---|
| Smooth Surface | 3.45 |
| Rectangular Groove (0.5 mm depth) | 3.58 |
| Rectangular Groove (1 mm depth) | 3.63 |
| Prismatic Groove (1.5 mm depth) | 3.76 |
| Grooving on both sides | 3.78 |

It has been observed that the maximum pressure is obtained for bearing having grooves on both sides and the second maximum for the prismatic grooves. However, it is difficult to engrave micro-cavities on both the journal and the bearing sides. This will make the economy infeasible and complicated.

## 11. RESULTS OBTAINED FROM NUMERICAL ANALYSIS

Since dynamic meshing in ANSYS made the problem analysis very complicated, further processing of the problem statement was carried out in MATLAB.

Different types of surface texturing have been used in the MATLAB environment for the analysis of non-dimensional load carrying capacity and friction variable for different values of non-dimensional dimple height and eccentricity ratio of hydrodynamic journal bearings.

**Cylindrical Textures**

The Sommerfeld number, Load Carrying capacity and Friction co-efficient is plotted for different dimple heights and eccentricity ratio in a cylindrical surface textured bearings. The table below lists the values for L/d = 1 and eccentricity ratio, ε=0.1

**Table 2** Different values of S, W and μ for different non-dimensional Dimple Height

| Non-dimensional Dimple Height, h | Sommerfeld Number, S | Non-dimensional Load Carrying Capacity, W | Friction Variable, μ |
|---|---|---|---|
| 0.1 | 1.1301 | 0.0469 | 22.0250 |
| 0.2 | 0.9142 | 0.0580 | 17.8253 |
| 0.3 | 0.6942 | 0.0764 | 13.5476 |
| 0.4 | 0.4885 | 0.1093 | 9.4899 |
| 0.5 | 0.3043 | 0.1743 | 5.9667 |
| 0.6 | 0.1633 | 0.3249 | 3.2238 |
| 0.7 | 0.0679 | 0.7818 | 1.3669 |
| 0.8 | 0.0155 | 3.4209 | 0.3443 |

www.ijprems.com
editor@ijprems.com

INTERNATIONAL JOURNAL OF PROGRESSIVE RESEARCH IN ENGINEERING MANAGEMENT AND SCIENCE (IJPREMS)

Vol. 02, Issue 09, September 2022, pp : 01-25

e-ISSN : 2583-1062

Impact Factor : 2.265

The Sommerfeld number, non-dimensional load carrying capacity and friction variable are tabled for different non-dimensional dimple height, h for a particular value of eccentricity ratio.

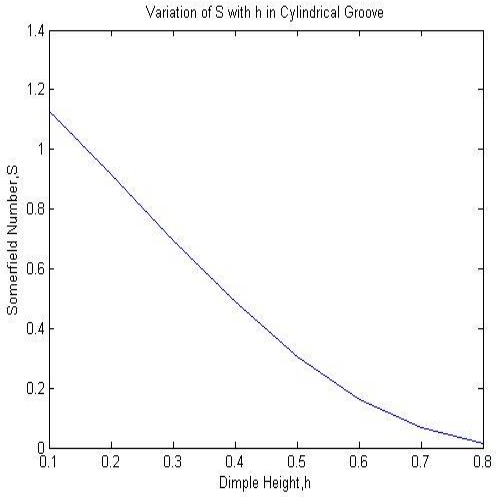


**Fig 22** Variation of S with h

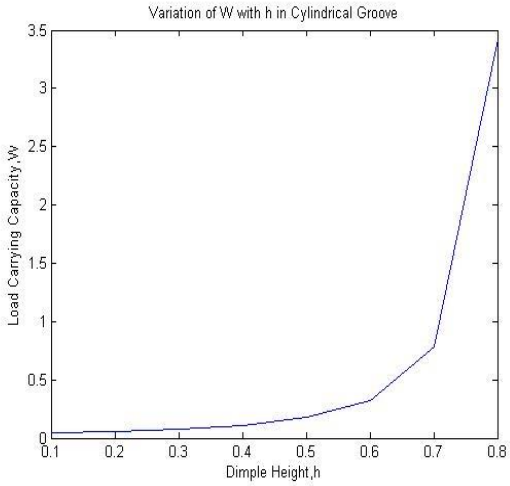


**Fig 23** Variation of W with h

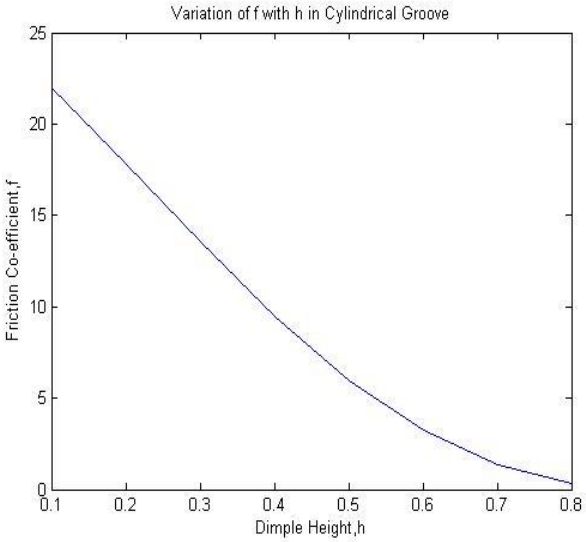


**Fig 24** Variation of μ with h

The data in the table 2 has been plotted for different non-dimensional dimple height. Fig 22 shows a decrease in the value of Sommerfeld number along with increasing height. There is a sharp increase in the non-dimensional load carrying capacity along the increasing dimple height (Fig 23). This is attributed to the fact that a little increase in the dimple height brings a huge change in the non-dimensional load carrying capacity.

The friction variable (Fig 24) decreases along the dimple height and this is a favorable condition for the operation of the bearing.

As the value of non-dimensional load carrying is maximum for the value of non-dimensional dimple height of 0.8, therefore keeping the value of h constant, different values of Sommerfeld number, non-dimensional load carrying capacity and friction variable for different eccentricity ratios are obtained as listed in Table 3 below.

**Table 3** Different values of S, W and μ for different Eccentricity Ratio

| Eccentricity Ratio, ε | Sommerfeld Number, S | Non-dimensional Load Carrying Capacity, W | Friction Variable, μ |
|---|---|---|---|
| 0.100 | 0.0155 | 3.4209 | 0.3443 |
| 0.125 | 0.0082 | 6.4655 | 0.2071 |
| 0.150 | 0.0035 | 15.0976 | 0.1169 |
| 0.175 | 0.0010 | 52.5846 | 0.0660 |
| 0.1875 | 0.00037 | 143.2704 | 0.0490 |

INTERNATIONAL JOURNAL OF PROGRESSIVE RESEARCH IN ENGINEERING MANAGEMENT AND SCIENCE (IJPREMS)

www.ijprems.com
editor@ijprems.com

Vol. 02, Issue 09, September 2022, pp : 01-25

e-ISSN : 2583-1062

Impact Factor : 2.265

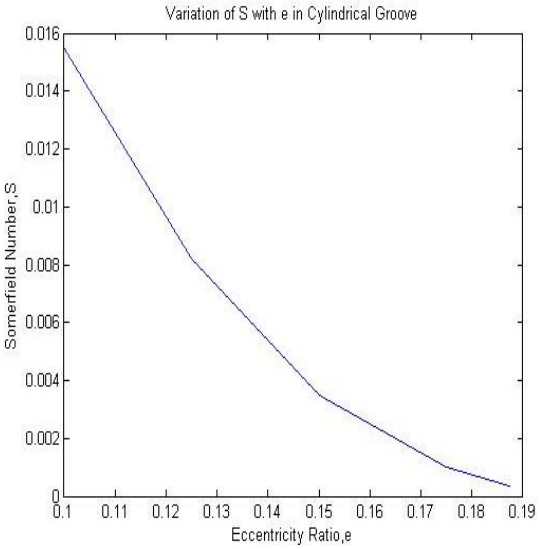


**Fig 25** Variation of S with ε

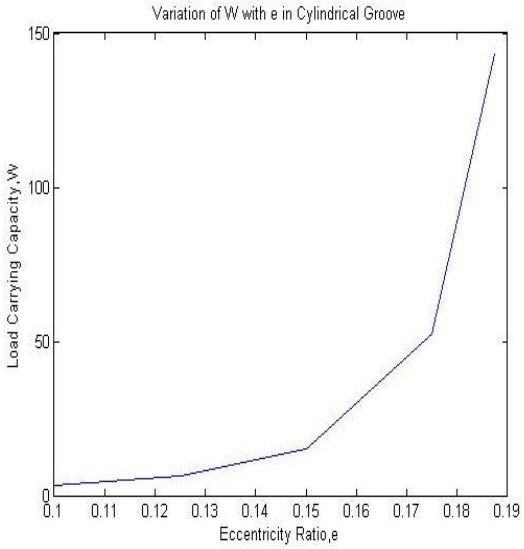


**Fig 26** Variation of W with ε

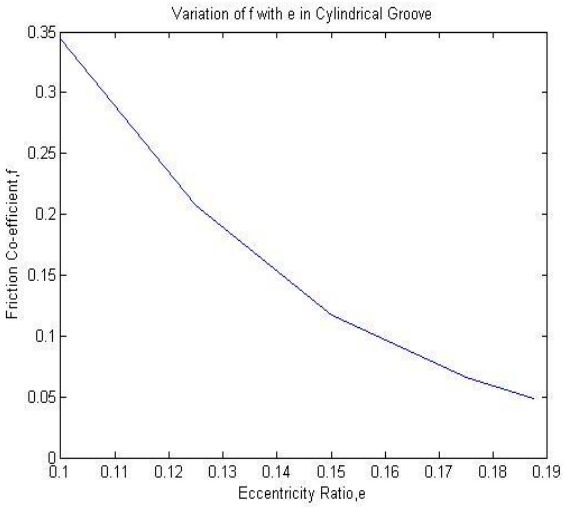


**Fig 27** Variation of μ with ε

The variation of Sommerfeld number shows a decreasing trend along with the friction variable as shown in Fig 25 and Fig 27. The non-dimensional load carrying capacity shows an increase, which is again a favorable condition for bearing load transmission. The non-dimensional load carrying capacity reaches a maximum value at ε=0.1875.

**Triangular Textures**

The Sommerfeld number, Load Carrying capacity and Friction co-efficient is plotted for different dimple heights and eccentricity ratio in a triangular surface textured bearings. The table below lists the values for L/d = 1 and eccentricity ratio, ε = 0.1

**Table 4** Different values of S, W and μ for different non-dimensional Dimple Height

| Non-dimensional Dimple Height, h | Somerfield Number, S | Non-dimensional Load Carrying Capacity, W | Friction Variable, μ |
|---|---|---|---|
| 0.1 | 1.2453 | 0.0426 | 24.2640 |
| 0.2 | 1.1309 | 0.0469 | 22.0398 |
| 0.3 | 0.9804 | 0.0541 | 19.1133 |
| 0.4 | 0.7906 | 0.0671 | 15.4219 |
| 0.5 | 0.5697 | 0.0931 | 11.1271 |
| 0.6 | 0.3453 | 0.3322 | 6.7631 |
| 0.7 | 0.1597 | 0.3453 | 3.1543 |
| 0.8 | 0.0461 | 1.1517 | 0.9439 |

www.ijprems.com
editor@ijprems.com

INTERNATIONAL JOURNAL OF PROGRESSIVE RESEARCH IN ENGINEERING MANAGEMENT AND SCIENCE (IJPREMS)

Vol. 02, Issue 09, September 2022, pp : 01-25

e-ISSN : 2583-1062

Impact Factor : 2.265

The data in the table 4 has been plotted for different non-dimensional dimple height. Fig 28 shows a decrease in the value of Sommerfeld number along with increasing height. There is a variable increase in the non-dimensional load carrying capacity along the increasing dimple height (Fig 28). This variable increase is attributed to the fact that the working fluid encounters sharp corners in triangular geometry.

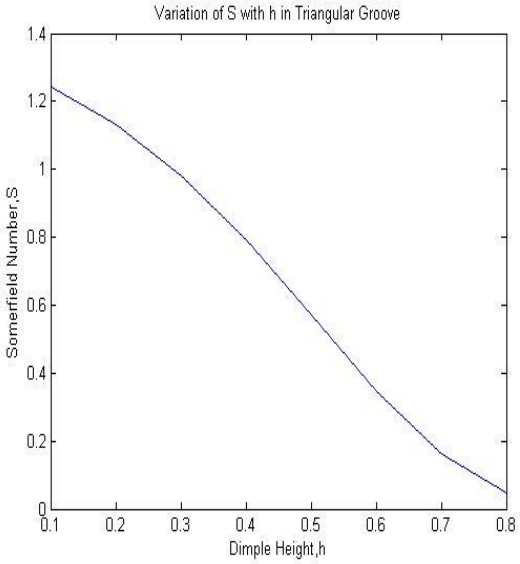


**Fig 28** Variation of S with h

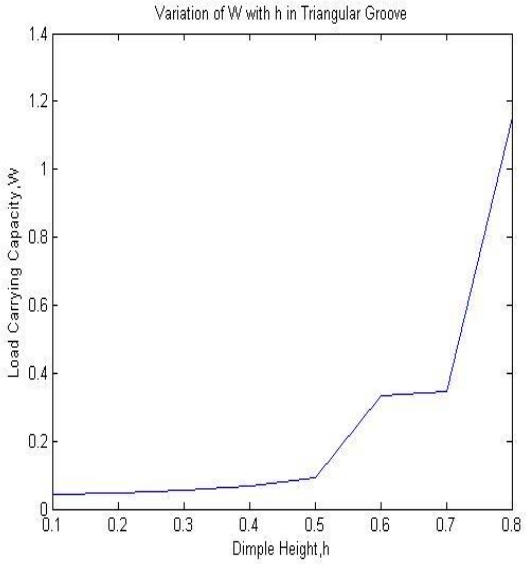


**Fig 29** Variation of W with h

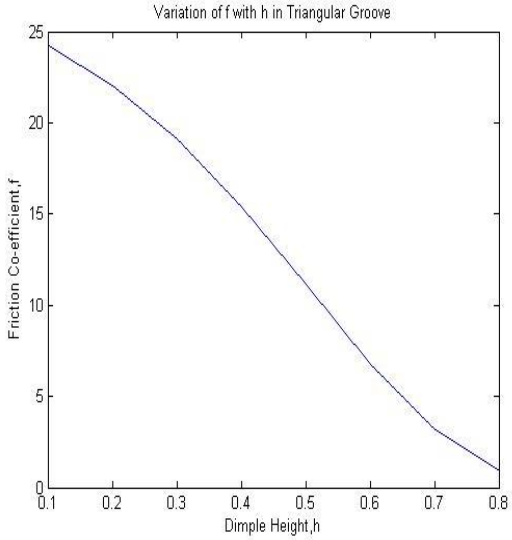


**Fig 30** Variation of μ with h

As the value of non-dimensional load carrying is maximum for the value of non-dimensional dimple height of 0.8, therefore keeping the value of h constant, different values of Sommerfeld number, non-dimensional load carrying capacity and friction variable for different eccentricity ratios are obtained as listed in Table 4.5 below.

**Table .5** Different values of S, W and μ for different Eccentricity Ratio

| Eccentricity Ratio, ε | Somerfield Number, S | Non-dimensional Load Carrying Capacity, W | Friction Variable, μ |
|---|---|---|---|
| 0.100 | 0.0461 | 1.1517 | 0.9439 |
| 0.125 | 0.0337 | 1.5720 | 0.7179 |
| 0.150 | 0.0251 | 2.1149 | 0.5616 |
| 0.175 | 0.0164 | 3.2252 | 0.3999 |
| 0.1875 | 0.0070 | 7.5870 | 0.1983 |

INTERNATIONAL JOURNAL OF PROGRESSIVE RESEARCH IN ENGINEERING MANAGEMENT AND SCIENCE (IJPREMS)

www.ijprems.com
editor@ijprems.com

Vol. 02, Issue 09, September 2022, pp : 01-25

e-ISSN : 2583-1062

Impact Factor : 2.265

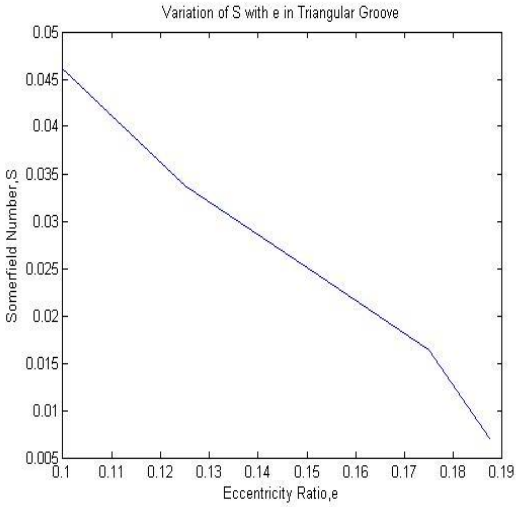


**Fig 31** Variation of S with ε

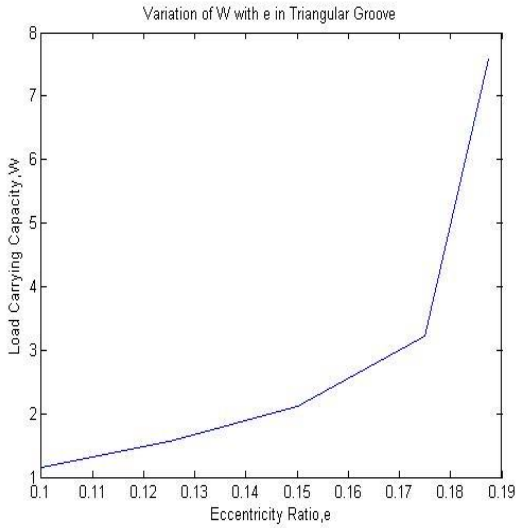


**Fig 32** Variation of W with ε

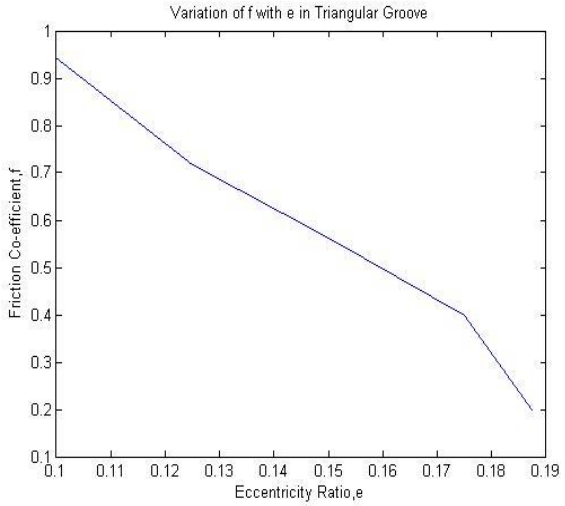


**Fig 33** Variation of μ with ε

The variation of Sommerfeld number shows a decreasing trend along with the friction variable as shown in Fig 31 and Fig 33. The non-dimensional load carrying capacity shows an increase, which is again a favorable condition for bearing load transmission. The non-dimensional load carrying capacity reaches a maximum value at ε=0.1875.

**Rectangular Textures**

The Sommerfeld number, Load Carrying capacity and Friction co-efficient is plotted for different dimple heights and eccentricity ratio in a rectangular surface textured bearings. The table below lists the values for L/d = 1 and eccentricity ratio, ε= 0.1

**Table.6** Different values of S, W and μ for different non-dimensional Dimple Height

| Non-dimensional Dimple Height, h | Somerfield Number, S | Non-dimensional Load Carrying Capacity, W | Friction Variable, μ |
|---|---|---|---|
| 0.1 | 1.2393 | 0.0428 | 24.1467 |
| 0.2 | 1.1147 | 0.0476 | 21.7248 |
| 0.3 | 0.9489 | 0.0559 | 18.4985 |
| 0.4 | 0.7397 | 0.0717 | 14.4311 |
| 0.5 | 0.5027 | 0.1055 | 9.8210 |
| 0.6 | 0.2772 | 0.1914 | 5.4329 |
| 0.7 | 0.1105 | 0.4799 | 2.1912 |
| 0.8 | 0.0244 | 2.1720 | 0.5153 |

www.ijprems.com
editor@ijprems.com

INTERNATIONAL JOURNAL OF PROGRESSIVE RESEARCH IN ENGINEERING MANAGEMENT AND SCIENCE (IJPREMS)

Vol. 02, Issue 09, September 2022, pp : 01-25

e-ISSN : 2583-1062

Impact Factor : 2.265

The data in the Table 6 has been plotted for different non-dimensional dimple height. Fig 34 shows a decrease in the value of Sommerfeld number along with increasing height. There is a variable increase in the non-dimensional load carrying capacity along the increasing dimple height (Fig 4.25).

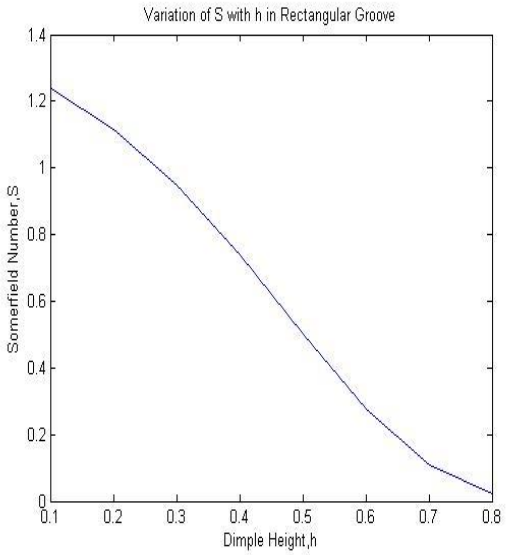


**Fig 34** Variation of S with h

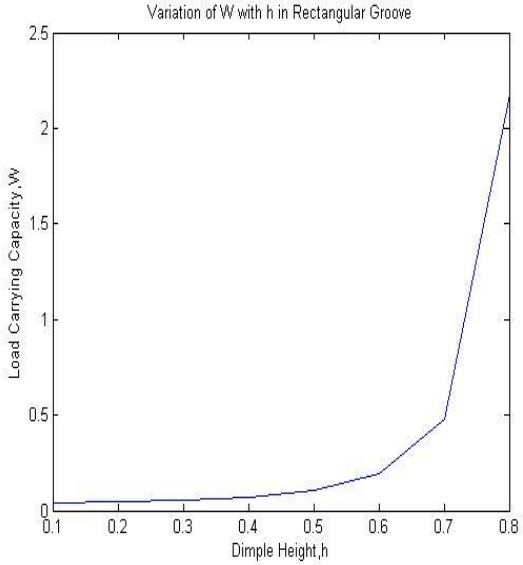


**Fig 35** Variation of W with h

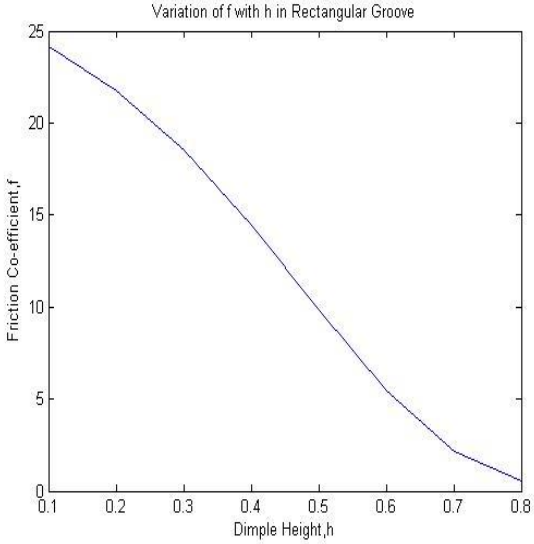


**Fig 36** Variation of μ with h

As the value of non-dimensional load carrying is maximum for the value of non-dimensional dimple height of 0.8, therefore keeping the value of h constant, different values of Sommerfeld number, non-dimensional load carrying capacity and friction variable for different eccentricity ratios are obtained as listed in Table 7 below.

**Table 7** Different values of S, W and μ for different Eccentricity Ratio

| Eccentricity Ratio, ε | Somerfield Number, S | Non-dimensional Load Carrying Capacity, W | Friction Variable, μ |
|---|---|---|---|
| 0.100 | 0.0244 | 2.1720 | 0.5153 |
| 0.125 | 0.0149 | 3.5503 | 0.3411 |
| 0.150 | 0.0093 | 5.7102 | 0.2405 |
| 0.175 | 0.0058 | 9.1948 | 0.1805 |
| 0.1875 | 0.0045 | 11.7268 | 0.1602 |

INTERNATIONAL JOURNAL OF PROGRESSIVE RESEARCH IN ENGINEERING MANAGEMENT AND SCIENCE (IJPREMS)

www.ijprems.com
editor@ijprems.com

Vol. 02, Issue 09, September 2022, pp : 01-25

e-ISSN : 2583-1062

Impact Factor : 2.265

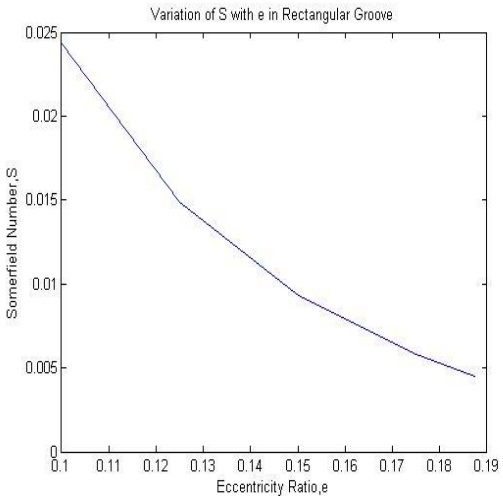


**Fig 37** Variation of S with ε

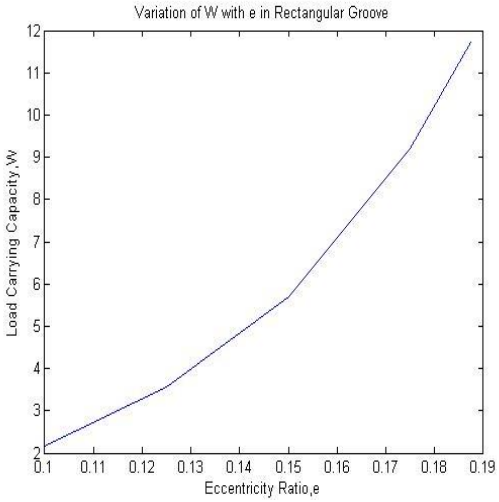


**Fig 38** Variation of W with ε

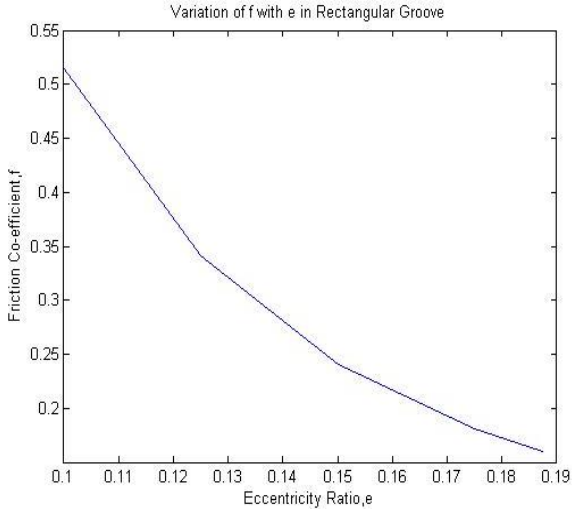


**Fig 39** Variation of μ with ε

The variation of Sommerfeld number shows a decreasing trend along with the friction variable as shown in Fig 37 and Fig 39. The non-dimensional load carrying capacity shows an increase, which is again a favorable condition for bearing load transmission. The non-dimensional load carrying capacity reaches a maximum value at ε=0.1875.

## 12. Comparative Study

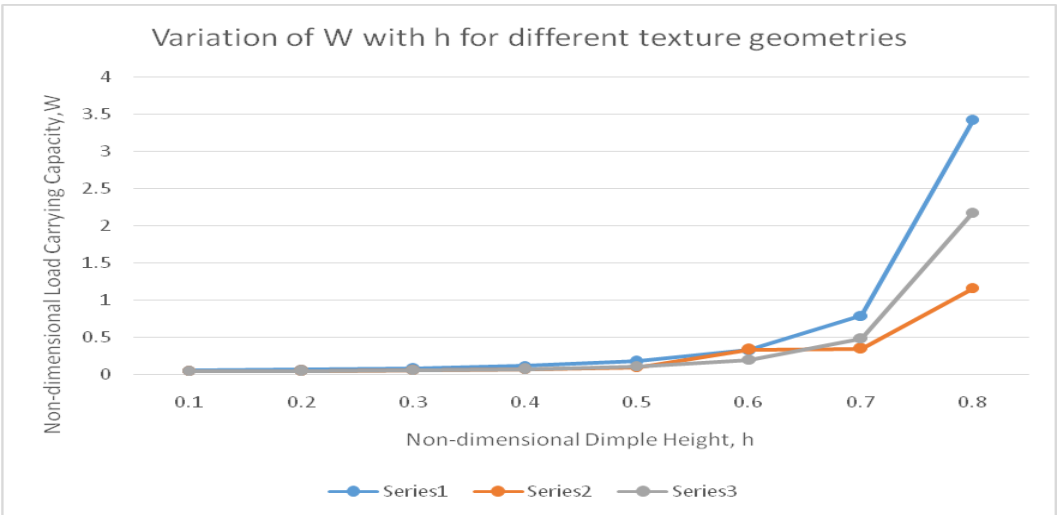


**Fig 40** Variation of W with h for different geometries

Fig 40 shows a comparative study of non-dimensional load carrying capacity for cylindrical (Series1), triangular (Series2) and rectangular (Series3) textures. It shows that the non-dimensional load carrying capacity is maximum for cylindrical textures followed by rectangular and triangular textures.

INTERNATIONAL JOURNAL OF PROGRESSIVE RESEARCH IN ENGINEERING MANAGEMENT AND SCIENCE (IJPREMS)

www.ijprems.com
editor@ijprems.com

Vol. 02, Issue 09, September 2022, pp : 01-25

e-ISSN : 2583-1062

Impact Factor : 2.265

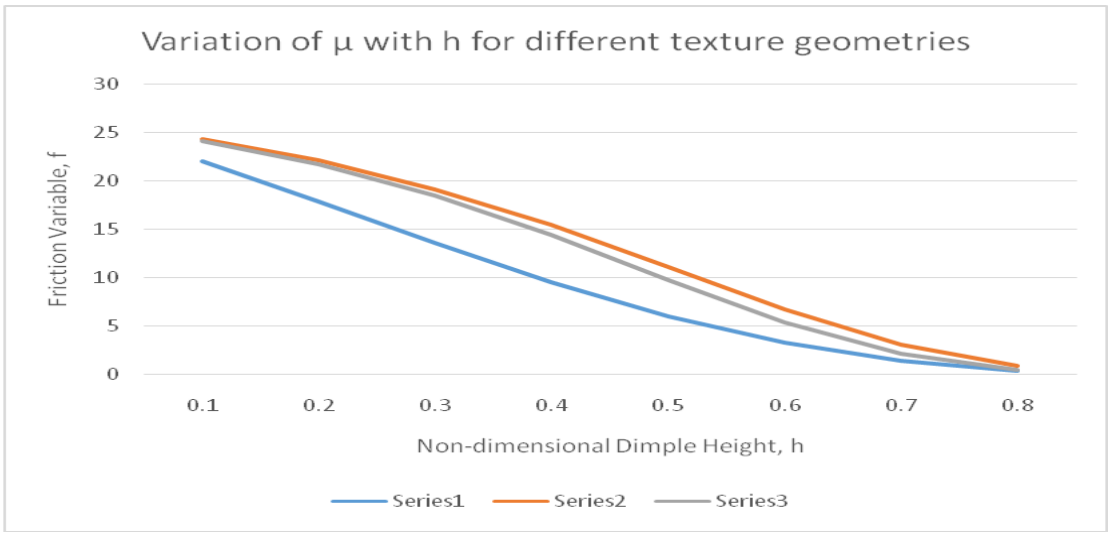


**Fig 41** Variation of μ with h for different geometries

The friction variable is least for cylindrical textures (Series1) and it goes on decreasing. The rectangular textures (Series3) follows and the decrement is least for triangular textures (Series2).

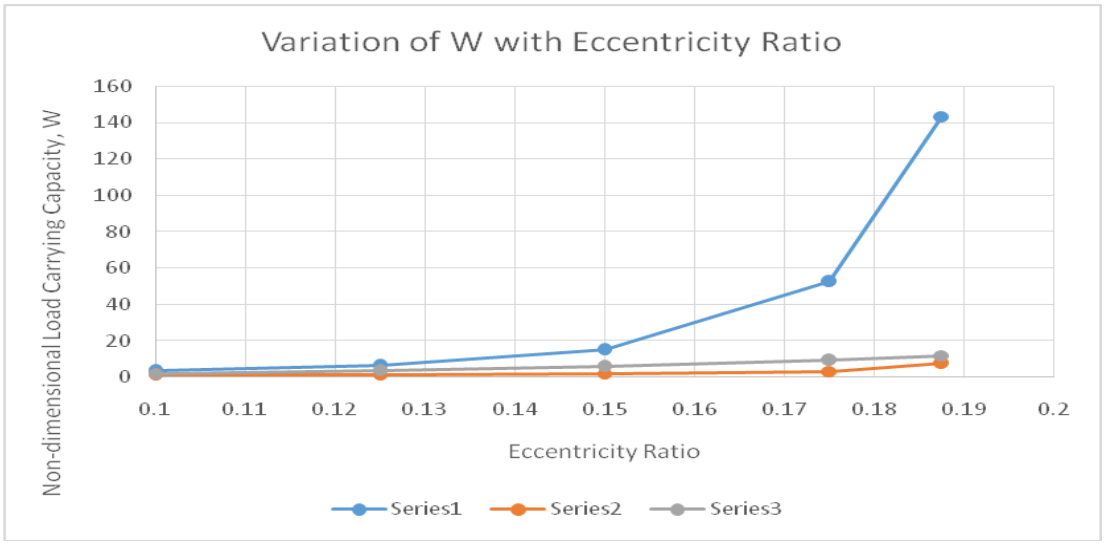


**Fig 42** Variation of W with ε for different geometries

Fig 42 shows a comparative study of non-dimensional load carrying capacity for cylindrical (Series1), triangular (Series2) and rectangular (Series3) textures with eccentricity ratio. It shows that the non-dimensional load carrying capacity is maximum for cylindrical textures followed by rectangular and triangular textures.

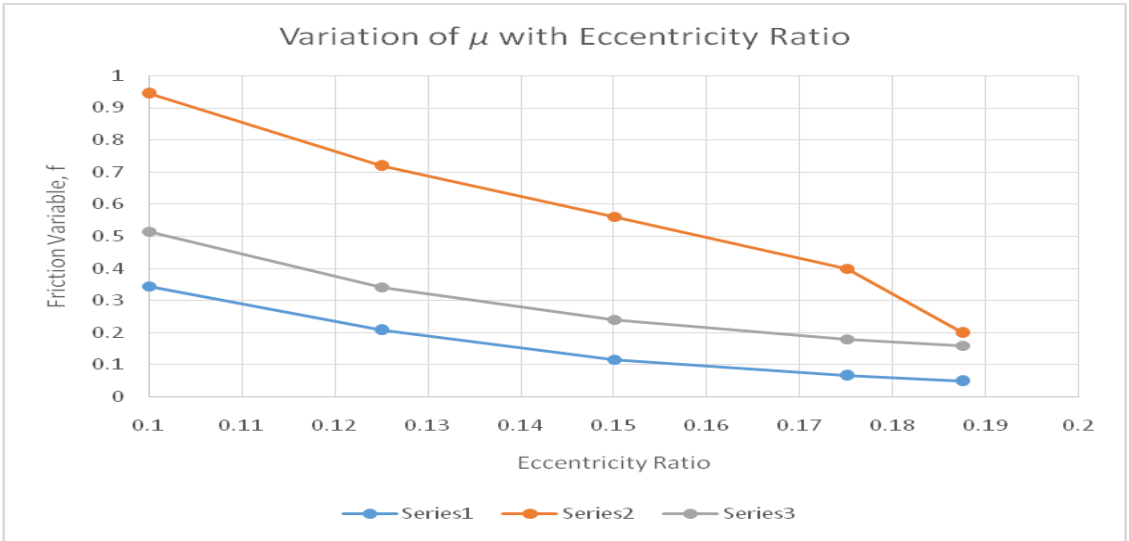


**Fig 43** Variation of μ with ε for different geometries

Fig 43 shows the variation of friction variable with eccentricity. The friction variable is least for cylindrical textures (Series1) and it goes on decreasing. The rectangular textures (Series3) follows and the decrement is least for triangular textures (Series2).

## 13. CONCLUSION

The ANSYS analysis show the maximum value of pressure developed for prismatic textures on bearing side and rectangular textures on journal side. The maximum pressure developed is $3.78x10^6$ Pa. The next highest pressure developed comes out in case of prismatic textures on the bearing side. The pressure developed comes out to be $3.76x10^6$ Pa. Since, texturing of both the journal and bearing is not metallurgically feasible, prismatic textures on the bearing side is considered to be the better kind of texture. But further analysis was not possible on ANSYS so numerical solution using MATLAB was considered.

The results obtained from MATLAB show the maximum value of load carrying capacity and minimum value of friction co-efficient in case of cylindrical grooving for a particular value of eccentricity ratio. The value of load carrying capacity and friction coefficient respectively become maximum and minimum for the non-dimensional dimple height of 0.8 and eccentricity ratio of 0.1875 in case of cylindrical grooving.

**Table 8** :Values of S, W and μ for dimple height of 0.8 in cylindrical grooving

| Non-dimensional Dimple Height, h | Sommerfeld Number, S | Non-dimensional Load Carrying Capacity, W | Friction Variable, μ |
|---|---|---|---|
| 0.8 | 0.0155 | 3.4209 | 0.3443 |

Table 8 shows the maximum values of the non-dimensional quantities at h=0.8.

With different textures and their parameters analyzed using MATLAB, the basic findings of the analysis are:

- At h=0.8 the non-dimensional load carrying capacity and friction variable become maximum and minimum respectively.
- Cylindrical textures carry maximum load and so is the better kind of texture amongst the rectangular and triangular textures.
- Cylindrical textures have the minimum value of friction variable and so this type of texture is the most economical according to our studies.

## 14. REFERENCES

[1] F.P. Snegovskii and N.G. Bulyuk. “Study of lubrication of sliding bearings with microgrooves on the sliding shafts”. TrenieiIznoa, pp. 4(2): 322-329, 1983.

[2] EtsionI.State of the art in laser surface texturing. ASME Journal of Tribology 2005;125:24853.

[3] Hamilton, D.B., Walowit, J.A., Allen, C.M.,(1966), “A Theory of lubrication by Microirregularities”, Transactions of ASME Journal of Basic Engineeering, 88, pp 177-185.

[4] Anno, J.N., Walowit, J.A, Allen, C.M., (1968), “Microasperity lubrication”, Journal of Basic engineering, Trans ASME, Ser. F, pp 351-355.

[5] Anno, J.N., Walowit, J.A, and Allen, C.M., (1969), “Load support and leakage from microasperity lubricated face seal”, Journal of Basic engineering, Trans ASME, Ser. F, pp 726-731.

[6] Etsion, I., Burstein, L., (1996),”A model for mechanical seals with regular microsurface structure”, Tribology Transactions, 39, 3, pp 677-683.

[7] Sinanoglu, Cem. "Investigation of load carriage capacity of journal bearings by surface texturing." Industrial Lubrication and Tribology (2009).

[8] Rahmani, Ramin, Iraj Mirzaee, Ayoub Shirvani, and HassanShirvani. "An analytical approach for analysis and optimisation of slider bearings with infinite width parallel textures." Tribology International 43, no. 8 (2010): 1551-1565.

[9] Tala-Ighil, Nacer, Michel Fillon, and Patrick Maspeyrot."Effect of textured area on the performances of a.hydrodynamic journal bearing." Tribology International 44, no. 3 (2011): 211-219.

[10] Cupillard, Samuel, Sergei Glavatskih, and M. J. Cervantes."Inertia effects in textured hydrodynamic contacts."Proceedings of the Institution of Mechanical Engineers, Part J: Journal of Engineering Tribology 224, no. 8 (2010): 751-756.

[11] Kango, S., R. K. Sharma, and R. K. Pandey. "Thermal analysis of microtextured journal bearing using non-Newtonian rheology of lubricant and JFO boundary conditions." Tribology International 69 (2014): 19-29.

[12] Gupta, K. Kumar, Raj Kumar, Harendra Kumar, and Medha Sharma. "Study on effect of surface texture on the performance of hydrodynamic journal bearing." International Journal of Engineering and Advanced Technology 3, no. 1 (2013): 49-54.

[13] Qiu, Mingfeng, Adis Delic, and Bart Raeymaekers. "The effect of texture shape on the load-carrying capacity of gaslubricated parallel slider bearings." Tribology Letters 48, no. 3 (2012): 315-327.

[14] Ganji, T. S., S. K. Kakoty, and R. K. Pandey. "Analysis on micro elliptical textured journal bearing." International Journal of Current Engineering and Technology 2, no. 2 (2014): 648-650.

[15] [15] Malik, Surajit, and Sashindra K. Kakoty. "Analysis of dimple textured parallel and inclined slider bearing." Proceedings of the Institution of Mechanical Engineers, Part J: Journal of Engineering Tribology 228, no. 12 (2014): 1343-1357